

~~Towards an understanding of~~ On the controls on relationship between $\delta\text{O}_2/\text{N}_2$ variability in and ice core records sheet surface conditions in Antarctica

Romilly Harris Stuart¹, Amaëlle Landais¹, Laurent Arnaud², Christo Buizert³, Emilie Capron², Marie Dumont⁴, Quentin Libois⁵, Robert Mulvaney⁶, Anaïs Orsi^{1,7}, Ghislain Picard², Frédéric Prié¹, Jeffrey Severinghaus⁸, Barbara Stenni⁹, and Patricia Martinerie²

¹Laboratoire des Sciences du Climat et de l'Environnement, LSCE-IPSL, CEA-CNRS-UVSQ, Univ. Paris-Saclay, 91190 Gif-sur-Yvette, France

²Université Grenoble Alpes, CNRS, INRAE, IRD, Grenoble INP, IGE, 38000 Grenoble, France

³College of Earth, Ocean, and Atmospheric Sciences, Oregon State University, Corvallis, OR 97331, USA

⁴Univ. Grenoble Alpes, Université de Toulouse, Météo-France, CNRS, CNRM, Centre d'Etudes de la Neige, 38000 Grenoble, France

⁵CNRM, Université de Toulouse, Météo-France, CNRS, Toulouse, France

⁶British Antarctic Survey, Natural Environment Research Council, Madingley Road, Cambridge CB3 0ET, UK

⁷The University of British Columbia, Department of Earth, Ocean and Atmospheric Sciences, Vancouver, Canada

⁸Scripps Institution of Oceanography, University of California, San Diego, La Jolla, CA 92093, USA

⁹Ca' Foscari University of Venice, Department of Environmental Sciences, Informatics and Statistics, Venezia, 30172, Italy

Correspondence: Romilly Harris Stuart (romilly.harris-stuart@lsce.ipsl.fr)

Abstract. Processes controlling pore closure are broadly understood yet defining the physical mechanisms controlling associated elemental fractionation remains ambiguous. Previous studies have shown that the pore closure process leads to a decrease in concentration of small-size molecules (e.g., H₂, O₂, Ar, Ne, He) in the ~~trapped~~-bubbles. Ice core $\delta(\text{O}_2/\text{N}_2)$ records – the ratio of O₂ to N₂ molecules in bubbles ~~trapped in ice cores~~ within the ice relative to the modern atmosphere – are therefore
5 depleted owing to this O₂ loss and show a clear link with local summer solstice insolation making it a useful dating tool. In this study, we compile $\delta(\text{O}_2/\text{N}_2)$ records from 14 polar ice cores and show a new additional link between $\delta(\text{O}_2/\text{N}_2)$ and local surface temperature and/or accumulation rate, ~~in addition to the influence of the summer solstice insolation. We argue that both~~
~~local climate-driven and insolation forcings are linked to the modulation of snow physical properties near the surface.~~ Using
10 the Crocus snowpack model, we perform sensitivity tests to identify the response of near-surface snow properties to changes in insolation, accumulation rate, and air temperature. These tests support a ~~mechanisms~~ mechanism linked to snow grain size, such that the larger the grain size for a given density, the stronger the pore closure fractionation, and hence, lower $\delta(\text{O}_2/\text{N}_2)$ values. ~~Our~~ Based on both snowpack model outputs and data compilation, our findings suggest that local accumulation rate and temperature should be considered when interpreting $\delta(\text{O}_2/\text{N}_2)$ as an insolation proxy.

1 Introduction

15 Ice cores store crucial information for our understanding of past climate variability and atmospheric composition. Interpreting ice core gas records first requires an understanding of the evolution of snow into ice via the firnification processes. Firn is the name given to the layer of ~~unconsolidated~~ consolidated snow which makes up the top 50-120m of ice sheets. Atmospheric air moves through porous networks within the firn until a critical depth (known as the lock-in depth) where vertical diffusion effectively stops, and ~~the pores gradually become sealed off from the atmosphere to form bubbles trapped within the ice. This depth is called the-~~ The lock-in depth (LID) and is largely controlled and the depth at which all pores are closed (close-off depth) are largely determined by local accumulation rate, temperature, and possibly the degree of density layering (Schwander et al., 1997; Martinerie et al., 1994; Mitchell et al., 2015). The region between the lock-in depth and close-off depth is known as the lock-in zone (LIZ).

~~Measurements of entrapped air can be used to reconstruct past atmospheric compositions, as well as to date the ice cores. One such dating technique, used primarily for deep ice cores from~~ Gas records from ice cores provide a vital dating tool, especially at low accumulation sites where other methods are unsuitable. One such tool is orbital dating, which ~~uses insolation curves at a given latitude enables certain gas records to be tuned to insolation curves~~ directly calculated from astronomical variables (Laskar et al., 2004). ~~Records of total air content (Raynaud et al., 2007), Ice core $\delta^{18}\text{O}_{\text{atm}}$ records ($\delta^{18}\text{O}$ of atmospheric O_2 (Extier et al., 2018), and)~~ are strongly correlated with precession (mid-June 65°N insolation) (Bender et al., 1994). $\delta^{18}\text{O}_{\text{atm}}$ provides a direct atmospheric signal which may ultimately be used to align different ice core records (Extier et al., 2018). The two alternative proxies for orbital dating are 1) total air content, which is anti-correlated with integrated summer insolation, i.e., the annual sum of daily insolation above a certain threshold (Raynaud et al., 2007), and 2) $\delta(\text{O}_2/\text{N}_2)$ (Kawamura et al., 2007; Suwa and Bender were found to be strongly-, which is anti-correlated with insolation curves, and thus, allow for ice core dating using peak matching techniques summer solstice insolation intensity (e.g., Kawamura et al., 2007; Bouchet et al., 2023). Unlike $\delta^{18}\text{O}_{\text{atm}}$, TAC and $\delta(\text{O}_2/\text{N}_2)$ reflect processes within the firn column making the records site specific. The term $\delta(\text{O}_2/\text{N}_2)$ – hereafter, simply $\delta\text{O}_2/\text{N}_2$ - describes the relative difference between the ratio of O_2 to N_2 molecules trapped within the ice and that of the standard atmosphere and is expressed in the delta notation commonly used for stable isotope ratios.

The use of $\delta\text{O}_2/\text{N}_2$ for ~~ice core~~ dating was first proposed by Bender (2002) after observations of an anti-correlation with local summer solstice insolation (hereafter SSI). Data from the Vostok ice core showed that high SSI corresponds to low $\delta\text{O}_2/\text{N}_2$ values ~~and vice versa (Bender et al., 1994) (Bender, 2002).~~ A similar relationship was then observed at ~~numerous~~ other sites such as Dome Fuji (Kawamura et al., 2007) and EPICA Dome C (Landais et al., 2012) in Antarctica, and GISP2 (Suwa and Bender, 2008b) in Greenland. Over orbital timescales, ~~the correlation between $\delta\text{O}_2/\text{N}_2$ and local SSI largely improved when matched is in anti-phase with local SSI when drawn~~ on the ice-age ~~timescale rather than the gas-age (Bender, 2002), suggesting that the impact of the insolation on the ice properties occurs at the surface rather than the pore closure depth.~~ chronology, indicating that the firn properties controlling the $\delta\text{O}_2/\text{N}_2$ fractionation are set near the surface. It is understood that temperature gradients are increased with high summer insolation leading to enhanced near surface snow metamorphism, thus increasing near-surface

grain size which persists throughout the firnification process down to the close-off depth (Bender, 2002; Severinghaus and Battle, 2006; Suwa

~

Parallel firn air studies of the open porosity revealed an enrichment in O_2 and other small molecules, such as Ar, Ne and He, compared to air within the closed porosity at the close-off depth (COD), providing further evidence of size-dependent fractionation during pore-closure (Battle et al., 1996; Huber et al., 2006; Severinghaus and Battle, 2006). While the physical mechanisms controlling the amount of fractionation are not fully understood, it is believed that ~~the main processes by which smaller molecules~~ smaller molecules (<3.6 Å diameter) escape during pore closure are: 1) via molecular diffusion through the ice lattice ~~, or permeation, resulting from (or permeation) driven by~~ pressure gradients between recently closed pores and neighbouring open pores (Ikeda-Fukazawa et al., 2004; Huber et al., 2006; Severinghaus and Battle, 2006), ~~and 2) diffusion through small openings in the ice matrix, with a threshold of 3.6 Å, allowing only molecules with a diameter below 3.6 Å to pass through (Huber et al., 2006; Severinghaus and Battle, 2006). Both processes are.~~ This process is facilitated by the pore network's capacity to export the fugitive gases back to the atmosphere, which is required for the observed depletion in ~~bulk ice~~ O_2 in bubbles (Fujita et al., 2009).

~~The simultaneous observations of O_2 depletion in entrapped air bubbles and O_2 enrichment in open porosity, alongside the strong correlation between SSI and $\delta O_2/N_2$ on the ice-age scale, led Bender (2002) to develop the hypothesis that the dependence of $\delta O_2/N_2$ on local insolation was the result of snow metamorphism near the surface. They, and many subsequent studies, proposed that strong summer insolation drives temperature gradient metamorphism, thus increasing near-surface grain size which propagates through the firn during the firnification process down to the COD (Bender, 2002; Severinghaus and Battle, 2006; Suwa~~
In addition, Fujita et al. (2009) proposed that $\delta O_2/N_2$ would be ~~decreased~~ low under high SSI conditions due to enhanced density stratification in the deep firn. They argue that ~~'summer' layers — layers~~ characterised by large grains and relatively low density in the deep firn ~~— ('summer' layers)~~ close-off deeper and take longer to do so than neighbouring ~~'winter' layers~~, which are denser and have smaller grains (Picard et al., 2012, 2016) ~~('winter' layers)~~. 'Summer' layers therefore remain permeable for longer, allowing the O_2 enriched air in open porosity to be exported to the atmosphere, and hence, reducing bulk ice $\delta O_2/N_2$ under high SSI conditions (Fujita et al., 2009). While the proposed mechanisms are posited to explain the SSI imprint on $\delta O_2/N_2$, they are also influenced by local climate conditions such as temperature ~~, accumulation rate and wind speed and~~ accumulation rate. Indeed, there is a substantial amount of evidence linking local climate conditions with both firn physical properties (McDowell et al., 2020; Casado et al., 2021; Inoue et al., 2023) ~~(Casado et al., 2021; Inoue et al., 2023)~~ and deep firn layering (Hörhold et al., 2011).

There is a growing body of evidence for a local climatic imprint on ice core $\delta O_2/N_2$ records. Firstly, spectral analysis has revealed climate related 100-ka cyclicity at EPICA Dome C (Bazin et al., 2016) ~~—although such a signal—~~. However, this 100 ka cyclicity is not apparent ~~at Dome F (Kawamura et al., 2007), in the Dome Fuji $\delta O_2/N_2$ record, which Kawamura et al. (2007) attribute to the idea that temperature and accumulation effects cancel each other out.~~ Secondly, millennial scale variability in $\delta O_2/N_2$ records from GISP2 appeared in-phase with local temperature fluctuations driven by Dansgaard-Oeschger events (Suwa and Bender, 2008b). In parallel contrast, Kobashi et al. (2015) evidenced an anti-phase effect of accumulation rate on $\delta Ar/N_2$ records at GISP2 over the last millennia 6000 years. Like O_2 , Ar is a smaller molecule than N_2 ~~so such~~ that the same

driving mechanisms are invoked for the $\delta\text{Ar}/\text{N}_2$ and $\delta\text{O}_2/\text{N}_2$ variations, but the $\delta\text{Ar}/\text{N}_2$ anomaly tends to be half as large as the $\delta\text{O}_2/\text{N}_2$ anomaly (Bender et al., 1995; Buizert et al., 2023). Kobashi et al. (2015) proposed a direct effect of accumulation rate or temperature on the $\delta\text{Ar}/\text{N}_2$ ($\delta\text{O}_2/\text{N}_2$) variations through the firn depth. The higher the accumulation rate or the lower the temperature, the higher the firn weight and hence the overloading pressures in microbubbles preferentially expelling Ar (O₂ and Ar) in the LIZ. ~~In contrast~~ Alternatively, Severinghaus and Battle (2006) proposed that the higher the accumulation rate, the more rapid the burial of bubbles, allowing less time for gases to escape during pore closure.

Using a combination of data compilation and snowpack modelling, we aim to develop our understanding of the formation of the ~~of~~ $\delta\text{O}_2/\text{N}_2$ records, ~~by first~~, by first determining the role of local climate parameters, accumulation rate and temperature, on $\delta\text{O}_2/\text{N}_2$ variability, and ~~second~~ subsequently identifying potential mechanisms related to snow physical properties using snowpack sensitivity tests. We use a compilation of datasets from 14 ice cores from both Antarctica and Greenland to identify spatial and temporal patterns in $\delta\text{O}_2/\text{N}_2$ depending on local surface conditions. The impacts of SSI and local climate on snow properties are then assessed using the SURFEX-ISBA-Crocus detailed snowpack model (Vionnet et al., 2012). We aim to constrain the influence of near-surface snow properties on $\delta\text{O}_2/\text{N}_2$ variability, potentially contributing to a mechanistic explanation for elemental fractionation during pore closure.

2 Methods

2.1 Ice core sites

We compiled $\delta\text{O}_2/\text{N}_2$ records from 18 ice cores from Antarctica and Greenland but use data from 14 of those sites for reasons explained in Section 2.42.2.3. Previously published data were measured on ice cores from: Dome Fuji (DF), EPICA Dome C (EDC), Greenland Ice Core Project 2 (GISP2), Law Dome DE08 and DSSW20k, North Greenland Ice core Project (NGRIP), Roosevelt Island Climate Evolution (RICE), Siple Dome (SD), South Pole (SP), Talos Dome (TALDICE), Vostok (VK), and the West Antarctic Ice Sheet Divide (WAISDWAIS) ice cores (references for all datasets are presented in Table S2). We also present unpublished data from Berkner Island (BI), EPICA Dronning Maud Land (EDML), Fletcher Promontory (FP), GISP2, James Ross Island (JRI), North Greenland Eemian Ice Drilling (NEEM), Skytrain Ice Rise (SIR) and Talos Dome (TALDICE) ice samples (overview of unpublished datasets in Table S1). Table 1 provides an overview of the site characteristics.

2.2 Analytical techniques for previously unpublished data

The previously unpublished $\delta\text{O}_2/\text{N}_2$ datasets were measured at the Laboratoire des Sciences du Climat et de l'Environnement (LSCE), with the addition of some GISP2 data measured at Scripps Institution of Oceanography (Scripps). At ~~LSCE, two techniques have been used to extract the trapped air from ice core samples and have been described in previous studies~~ (Landais et al., 2003; Capron et al., 2013; Bazin et al., 2016) both LSCE and Scripps, gases are extracted from the ice using a melt-refreeze technique based on the method described by Sowers et al. (1989) with modifications to the LSCE method as described by Landais et al. (2003), and to the Scripps method as outlined in Petrenko et al. (2006). In short, ~~the first uses a~~

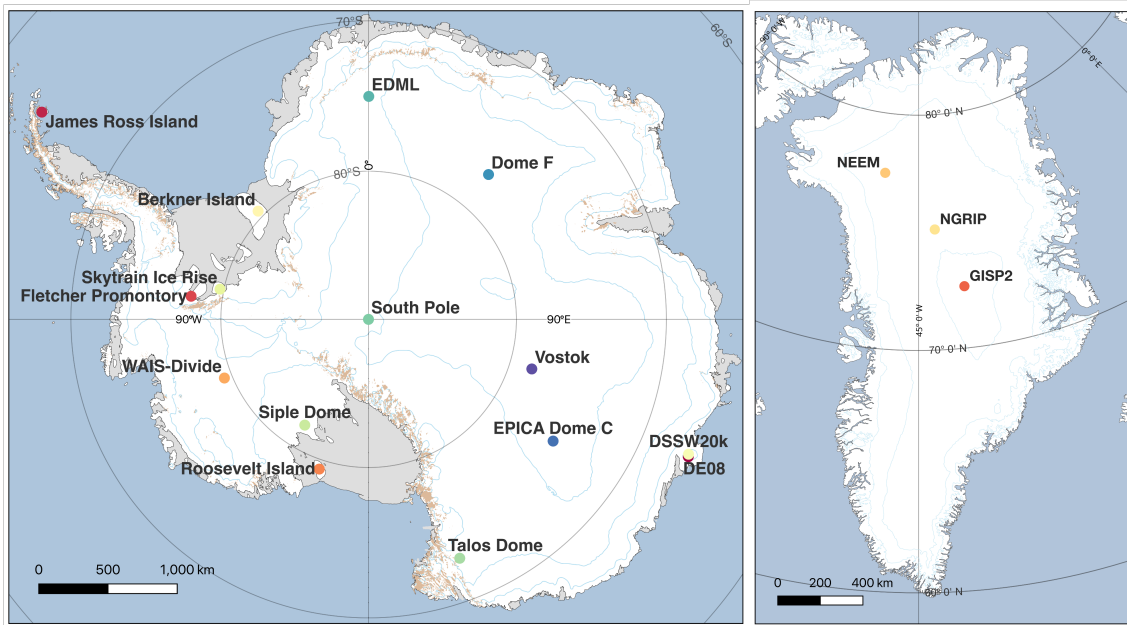


Figure 1. Locations of each ice core site initially included in our study. ~~Maps were made in QAntarctica and QGreenland~~ (Matsuoka et al., 2018; Moon et al., 2023).

~~melt-refreeze technique where~~ ice samples are placed into glass flasks at -20°C while the atmospheric air is evacuated. Samples are then left to slowly melt to release the trapped gases, before ~~the samples are refrozen with liquid nitrogen being refrozen~~. The extracted air samples are then ~~individually introduced into the line and~~ passed through a CO_2 and water vapour trap, before being trapped in the stainless-steel dip-tube submerged in liquid helium (Landais et al., 2003). ~~The second uses a~~. An alternative semi-automated extraction (melt-extraction) line technique is now more commonly used at LSCE which removes the need for refreezing of the samples (Capron et al., 2010; Bazin et al., 2016). For all datasets (Bazin et al., 2016; Bouchet et al., 2023).

2.2.1 New $\delta\text{O}_2/\text{N}_2$ measurements

120 Samples from the following sites were measured at LSCE, ~~the average analytical uncertainty~~ France on a 10-collector Thermo Delta V Plus, unless otherwise stated. In all cases, the values used in this study are the average of at least two replicate measurements and have an average analytical uncertainty of 0.5‰ for $\delta\text{O}_2/\text{N}_2$ is 0.5‰ .

125 ~~Unpublished data from the GISP2 core were measured at the Ice Core Noble Gas Laboratory of the Scripps Institution of Oceanography using the melt and refreeze technique (Sowers et al., 1989; Petrenko et al., 2006). Additional information on the GISP2 measurements is available in Martin et al. (2023) where they use the $\delta^{15}\text{N}$ of N_2 from the same samples. An overview of all datasets, both previously published and unpublished, can be found in Table S1 and Table S2, respectively.~~

Table 1. Overview of ice core site characteristics. The ~~final three columns show the average annual accumulation rate~~ acronym BCTZ stands for brittle-cla
~~surface snow density at each site~~ COD stands for present-day conditions ~~close-off depth~~.

height	Site	Latitude	Latitude	Longitude	Longitude	Elevation	Elevation	Brittle-zone BCTZ ^a	Accumulat
~		(°NS)	(°E)			(m)	(m)		
BI	Berkner Island ¹	-79.55	79.55	-45.68		890		450-940 ¹	
DF	Dome Fuji ²	-77.32	77.32	39.7		3810		450-1200	450-1200
EDC	EPICA Dome C ³	-75.1	75.1	123.35		3233		600-1200	600-1200
EDML	EPICA Dronning Maud Land ⁴	-75	75	0.04		2892		500-1050	800-1200
FP	Fletcher Promontory ⁵	-77.9	77.9	-82.61		873			8
GISP2	GISP2 ⁶	72.6	-72.6	-38.5		3200		650-1400	650-1400
JRI	James Ross Island ⁷	-64.2	64.2	-57.69		1542			8
LD-DE08	DE08 ⁸	-66.72	66.72	113.2		1250		525-1200	
LD-DSSW20k	DSSW20k ⁹	-66.77	66.77	112.81		1370			
NEEM	NEEM ¹⁰	77.45	-77.45	-51.6		2450		609-1281	600-1200
NGRIP	NGRIP ¹¹	75.1	-75.1	-42.32		3090		790-1200	790-1200
RICE	Roosevelt Island ¹²	-79.36	79.36	-161.71		550		650-1300	
SD	Siple Dome ¹³	-81.65	81.65	-148.81		621		400-1000	
SIR	Skytrain Ice Rise ¹⁴	-79.74	79.74	-78.55		784			21
SP	South Pole ¹⁵	-89.99	89.99	-98.16		2835		619-1078	619-1078
TALDICE	Talos Dome ¹⁶	-72.82	72.82	159.07		2315		667-1002	667-1002
VK	Vostok ¹⁷	-78.47	78.47	106.87		3488		300-720	500-1250
WAISD	WAIS-Divide ¹⁸	-79.47	79.47	-112.09		1766		650-1300	1100-1200

¹Mulvaney et al., 2007^{a,b,c,d}; ²Oyabu et al., 2023^a; Oyabu et al., 2021^a; Fujita et al., 1998^{b,c}; Watanabe et al., 1997^d; ³Fujita et al., 1998^a; Parrenin et al., 2007^a; ⁴Frezzotti et al., 2004; ⁵Stenni et al., 2004; ⁶Oerter et al., 2000; ⁷EPICA community members, 2006; ⁸Mulvaney et al., 2014; ⁹Alley et al., 1993; ¹⁰Alley et al., 1993^a; Neff, 2014^a; Oerter et al., 2000^{b,d}; EPICA community members, 2006^c; ⁵Mulvaney et al., 2014^{a,b,c,d}; ⁶Gow et al., 1997^a; Alley et al., 1993^b; Alley et al., 1993^c; Capron et al., 2013^{b,c}; ⁸Rubino et al., 2019^a; Etheridge and Wokey, 1988^{b,c}; Etheridge et al., 1996^d; ⁹Rubino et al., 2019^a; Morgan et al., 2012^a; Buizert et al., 2012^{b,c,d}; ¹¹NGRIP project members, 2004^{a,b,c}; Martinier et al., 2009^d; ¹²Neff, 2014^a; Winstrup et al., 2019^b; Bertler et al., 2017^c; ¹³Alley et al., 1993^a; ¹⁴Mulvaney et al., 2021^{a,b,c}; ¹⁵Lazzara et al., 2012^a; Mosley-Thompson et al., 1999^b; ¹⁶NGRIP project members, 2004; ¹⁷Winstrup et al., 2019; ¹⁸Bertler et al., 2018; ¹⁹Severinghaus et al., 2001; ²⁰Hamilton, 2002; ²¹Alley et al., 1993^a; ²⁴Mosley-Thompson et al., 1999; ²⁵Stenni et al., 2002; ²⁶Arnaud et al., 2000; ²⁷Fegyveresi et al., 2011. All brittle zones are those presented by Neff et al., 2014^a; Severinghaus et al., 2001^{b,c,d}; ¹⁴Mulvaney et al., 2021^{a,b,c}; Hoffmann et al., 2022^d; ¹⁵Lazzara et al., 2012^a; Mosley-Thompson et al., 1999^b; ¹⁷Uchida et al., 1994^a; Petit et al., 1999^{b,c}; Cuffey and Paterson, 2010^d; ¹⁸Fegyveresi et al., 2011^{b,c}; Battle et al., 2011^d.

2.2.2 New $\delta O_2/N_2$ measurements

Berkner Island

Measurements were performed on bubbly ice from the Berkner Island BI ice core every 55 cm (every bag) between 631 m and 680m, corresponding to 10,269—21,269—21,350 yr BP (Capron et al., 2013). Replicate samples were prepared at

LSCE using the melt-refreeze method ~~and measured on a 10-collector Thermo Delta V Plus~~ between March 2010 and March 2011.

EDML

135 Nine samples were measured on bubbly ice from the EDML ice core over five depth levels between ~~328-473~~328-473 m (327.8 m (4.51 ka BP), 354.2 m (4.95 ka BP), 381 m (5.43 ka BP), 467 m (7.04 ka BP), and 473 m (7.16 ka BP)) (Bazin et al., 2013). The samples were prepared using the melt-refreeze method ~~and measured on the 10-collector Thermo Delta V Plus~~ at LSCE. ~~Where possible, the final value of each sample is the average of two replicate measurements at each depth level.~~

Fletcher Promontory

140 In January 2015, 39 depth levels were measured from the ~~Fletcher Promontory~~FP ice core, retrieved in 2012. Measurements were performed approximately every 3 m starting at 289 m down to 388 m. There is currently no published age-scale for the FP ice core. All samples were prepared using the melt extraction method ~~and then measured using a 10-collector Thermo Delta V Plus as LSCE. The final value of each sample is the average of at least two replicate measurements at each depth level.~~

145 ~~GISP2New GISP2 $\delta\text{O}_2/\text{N}_2$ data were analysed at Scripps Institution of Oceanography from 643 depths between 1740 and 2400 m (13 to 50 ka BP), with the $\delta^{15}\text{N}$ data from these analyses reported previously (Martin et al., 2023). Most of the samples were analysed in replicate. Measurements were performed in several campaigns between 2017-2020 and referenced to La Jolla pier air. Measurements were performed using a melt-refreeze method (Petrenko et al., 2006).~~

James Ross Island

150 Between February and March 2011, measurements were performed at 16 depth levels on the ~~James Ross Island Ice~~JRI ice core. The depth resolution varied between ~~2-50~~2-50 m starting at 52 m until 363 m corresponding to 0.03-14.3 ka BP (Mulvaney et al., 2012). Samples were prepared using the melt extraction method ~~and then measured using a 10-collector Thermo Delta V Plus as LSCE. The final value of each sample is the average of at least two replicate measurements at each depth level.~~

155 *NEEM*

Clathrate ice from the NEEM ice core was measured between February and April 2011, a year after the core was retrieved. A total of 119 depth levels were sampled were measured at varying resolutions over the following intervals: 55cm intervals (every bag) between ~~1757-1773~~1757-1773 m (38.127-~~39.735~~39.735 ka B2k), 5.5 m intervals (every 10 bags) between 2205 and 2370 m (108.56-~~120.237~~120.237 ka B2k), every 2 bags from 2375-2434 m (no published age-scale available below these depths), and 5.5 m intervals (every 10 bags) between 2436 and 2519 m (Gkinis et al., 2021; Rasmussen et al., 2013). In total, samples from 119 depth levels were prepared using the melt-refreeze method ~~and measured using a 10-collector Thermo Delta V Plus as LSCE. The final value of each sample is the average of at least two replicate measurements at each depth level.~~

165 Measurements were performed on bubbly ice from the ~~Skytrain Ice Rise~~ SIR ice core between March and April 2021. Samples were taken sporadically (~~1-151-15~~ m intervals) at 16 depth levels between 307 and 436 m depth (4.707-~~11.696~~ -11.696 ka BP) (Mulvaney et al., 2023). Each sample was prepared at LSCE using the melt extraction method ~~and subsequently measured on a 10-collector Thermo Delta V Plus. The final value of each sample is the average of at least two replicate measurements at each of the 16 depth levels.~~

170 *TALDICE*

Numerous measurements have been ~~done~~ performed on bubbly and clathrate ice from TALDICE between 2008 and 2022 at LSCE. A total of 308 depth levels were measured at varying intervals starting at 155 m down to 1617 m. Published age-scales reach 1548 m, giving an age range of 1.55-~~343-343~~ ka for TALDICE samples (Buiron et al., 2011; Crotti et al., 2021). All samples were prepared using the melt extraction technique ~~and measured on the 10-collector Thermo Delta V Plus~~. Some measurements between ~~1356-1620~~ 1356-1620 m depth have been published previously and are available in Crotti et al. (2021).

Samples from GISP2 were measured at Scripps Institution of Oceanography on a 3kV Thermo Finnigan Delta V plus 217 dual inlet IRMS (isotope ratio mass spectrometer).

GISP2

180 Measurements were performed on samples from 643 depths between 1740 and 2400 m (13–50 ka BP) over several measurement campaigns between 2017–2020 and referenced to La Jolla pier air. The melt-refreeze technique was used for gas extraction, and the $\delta^{15}\text{N}$ of N_2 data from these samples were previously reported (Martin et al., 2023). Again, the majority of the samples were analysed in replicate.

2.2.2 Corrections

185 Chemical slope and pressure imbalance corrections are applied to the measurements during data processing (Landais et al., 2003). In addition, all data are corrected for gravitational fractionation in the firn using $\delta^{15}\text{N}$ of N_2 from the same samples.

$$\delta_{\text{O}_2/\text{N}_2 \text{ grav}} = \delta_{\text{O}_2/\text{N}_2} - 4 \cdot \delta^{15}\text{N} \quad \delta_{\text{O}_2/\text{N}_2 \text{ grav.corr.}} = \delta_{\text{O}_2/\text{N}_2} - 4 \cdot \delta^{15}\text{N} \quad (1)$$

Gas loss effects during ~~coring and~~ ice core storage are well documented to modify $\delta_{\text{O}_2/\text{N}_2}$, causing significant depletion in O_2 in clathrate ice stored above -50°C (Ikeda-Fukazawa et al., 2005; Kawamura et al., 2007; Landais et al., 2012). Ikeda-
190 Fukazawa et al. (2005) proposed ~~an equation to correct for a correction for storage~~ gas loss effects ~~during storage at different temperatures~~ as a function of temperature and time. However, given the incomplete storage history for all ice cores we do not attempt to correct for storage gas loss, but rather define rejection criteria outlined in Section 2.2.3.

2.2.3 Data rejection criteria

195 ~~At the transition zone between bubbly ice and clathrate ice (hereafter the brittle zone) strong~~ Ice core storage histories need to be considered before interpreting the data to account for post-coring gas loss effects which disturb the signal (Section 2.2.2). Successive $\delta\text{O}_2/\text{N}_2$ measurements from TALDICE and GISP2 clathrate ice samples show strong depletion of O_2 through time (Supplement S1), which is consistent with observations from EDC (Bouchet et al., 2023). We systematically reject measurements from clathrate ice stored at -20°C for over 3 years, or at -36°C for more than 4 years. Bubbly ice stored at these same temperatures appear to be mostly unaffected by gas loss (Supplement S1), with the exception of Vostok (Bender, 2002).

200 Several measurements were performed on ice within the bubble-clathrate transition zone (BCTZ: where the high hydrostatic pressure in the bubbles cause entrapped gases to form clathrate hydrates (Schaefer et al., 2011)). At these depths, elemental fractionation occurs ~~whereby the air in the gas phase has a very different composition to that in the clathrate hydrates due to some gas species being preferentially incorporated into the clathrate structures (Ikeda-Fukazawa et al., 2001)~~, thus making the interpretation of gas measurements unreliable ~~at these depths (Bender, 2002). Measurements from brittle ice tend to be characterised as having (Bender, 2002).~~ While brittle ice is reported at intermediate depth sites, such as BI, JRI, DE08, DSSW20k, RICE, and SD, we do not consider these BCTZs due to the absence of clathrate hydrates (Neff, 2014; Rubino et al., 2019). Measurements from the BCTZ may either have increased mean $\delta\text{O}_2/\text{N}_2$ (usually in excess of 0‰) ~~and/or~~ strong data scattering, expressed as a high standard deviation. ~~All measurements from Berkner Island fall within the reported brittle zone but show no scattering, and are therefore included in our analysis. This is also observed at other sites — where some depths defined as the brittle zone show no evidence of scattering — and is expected to be due to the approximation of the brittle zone depths. (Oyabu et al., 2021).~~ To avoid adding biases to our analysis, measurements from ~~brittle ice from all other sites are removed, leaving the measurements from bubbly ice above, and the clathrate ice below the brittle zone~~ BCTZ are removed. Additional scattering in elemental ratios, characterised by a standard deviation of 6.2‰ compared to 1.8‰ in ~~non-brittle pure bubble and clathrate~~ ice, is observed below the ~~brittle zone in the WAIS Divide record between 1300–1500~~ BCTZ in the WAIS record ~~between 1300–1500 m (Shackleton, 2019). Similar effects were observed on have been documented in the EDC and TALDICE ice cores (Lüthi et al., 2010), and the Dome Fuji ice core (Oyabu et al., 2021). Data influenced by this scattering effect was~~ were also removed from our analysis, ~~followed by the removal of outliers from the cleaned datasets.~~

215 ~~The different storage histories of ice used for each measurement campaign need to be considered before interpreting the data to account for gas loss effects (Section 2.2.2). Successive $\delta\text{O}_2/\text{N}_2$ measurements from TALDICE and GISP2 clathrate ice samples show strong depletion of O_2 through time (Supplement S1), which is consistent with observations from Dome C (Bouchet et al., 2023). Having separated the datasets into bubbly ice and clathrate ice — by taking the data above and below the brittle zone — we systematically reject measurements from clathrate ice stored at -20°C for over 3 years, or at -36°C for more than 4 years. Bubbly ice stored at these same temperatures appear largely unaffected by gas loss (Supplement S1), with the exception of Vostok (Suwa and Bender, 2008a). Applying these criteria to the datasets results~~ We note that these criteria ~~result~~ result in the removal of all data from NGRIP and Vostok, as well as sections of data from other sites. ~~(see Supplement S1 for overview).~~ The remaining 14 datasets are presented in Table 3 and were used to analyse the drivers of $\delta\text{O}_2/\text{N}_2$ variability. ~~We also exclude FP and SIR due to limited availability of accumulation rate and temperature records.~~

225

2.3 Modelling near-surface snow properties

The second component of our study addresses the modelled response of snow physical properties to perturbations in SSI, accumulation rate, and temperature with the aim of identifying which properties may be influencing elemental fractionation during pore closure. We use the SURFEX-ISBA-Crocus detailed snowpack model (Crocus hereafter) to simulate snowpack evolution (Vionnet et al., 2012). Crocus simulates changes in snow physical properties induced by surface metamorphism and the evolution of these properties with depth. The model is forced by ERA5 reanalysis data (Hersbach et al., 2020), and the snowpack is initialised with measurements of snow density, effective optical radius of snow grains and snow temperature. Optical radius is defined as the radius which snow grains would have for their surface area-to-volume ratio if they were spherical (Domine et al., 2006). Optical radius is thus directly linked to specific surface area (SSA), defined as the surface area of snow at the ice-air interface per unit mass (units $\text{m}^2 \text{kg}^{-1}$) (Legagneux et al., 2002), via the following equation:

$$\text{SSA} = \frac{3}{r_{\text{opt}} \cdot \rho_{\text{ice}}} \frac{3}{r_{\text{opt}} \cdot \rho_{\text{ice}}} \quad (2)$$

Where r_{opt} is the optical radius and ρ_{ice} is the density of ice (Gallet et al., 2014). We use this model to assess changes in snow physical properties near the surface which are invoked to explain $\delta\text{O}_2/\text{N}_2$ variability. Dome C is used as the test site given the abundance of snowpack observations as well as high resolution $\delta\text{O}_2/\text{N}_2$ data.

2.3.1 Crocus model description

Crocus is a 1-dimensional model which simulates the evolution of snow properties with time and depth on a layer-by-layer basis, i.e., in a Lagrangian framework (Vionnet et al., 2012). A detailed description of the model can be found in Vionnet et al. (2012). Briefly, the initial number of layers is defined by the user, with the thickness of each layer allowed to change along the simulation (layer thickness ranging from millimetres to metres thick). The maximum number of layers available in the model was increased from 50 (Libois et al., 2014) to 80 to account for the higher number of thin layers forming at Dome C than at Alpine sites. Once the simulated snowpack consists of 80 layers, the aggregation scheme merges internal neighbouring layers with similar properties allowing a new surface layer to form. The key physical processes incorporated into Crocus for dry snow conditions are accumulation of snowfall, snow metamorphism, compaction of snow by the wind, compaction due to the weight of the overlying layers, absorption of solar radiation, heat diffusion, and surface energy budget.

For our study, two fundamental user-defined model components are the snow metamorphism and radiative transfer schemes. We use the semi-empirical model from Flanner and Zender (2006) (F06) for the metamorphism scheme which describes the evolution of optical radius with time. F06 was found to be the most appropriate formulation for Dome C conditions (Carmagnola et al., 2014; Libois et al., 2014). To successfully reproduce the snow temperature profile – vital for realistically simulating snow metamorphism – the Two-stream Radiative Transfer in Snow model (TARTES) is used to account for vertical distribution of absorbed solar radiation in the snowpack (Libois et al., 2013). TARTES also considers the effect of impurities on snow temperature via albedo. For Dome C, we include black carbon content which is set to 3 ng g^{-1} (Warren et al., 2006;

260 Libois et al., 2015). ~~In this study,~~ Here we assess the simulated snow density, snow temperature, and snow SSA from Crocus model outputs.

2.3.2 Dome C specific Crocus configuration

Crocus was initially developed for alpine or sub-polar regions with seasonal snowpacks. Libois et al. (2014) modified multiple components of the Crocus model to improve its suitability to high latitude sites with low accumulation rates - specifically for
265 Dome C. The modifications are extensively described in Libois et al. (2014) and were implemented into the current version of Crocus for this study. The changes are as follows:

1. *Fresh snow properties*: The parameterisation of fresh snow density is based on temperature and wind-speed which results in an unrealistically low density for Dome C ~~conditions~~ (50kg m^{-3}). Fresh snow density is fixed to a minimum of 170kg m^{-3} , ~~the lowest fifth percentile from Dome C observations~~ (Libois et al., 2014). Similarly, fresh snow SSA
270 is set to $100\text{m}^2\text{kg}^{-1}$ instead of $65\text{m}^2\text{kg}^{-1}$ used in the standard version of the model (Grenfell et al., 1994; Libois et al., 2014).
2. *Wind-induced compaction*: At low-accumulation sites, ~~the snow can remain~~ snow remains at the surface for prolonged periods of time. The long exposure time to surface winds facilitates compaction, and hence, increases density. The maximum surface snow density is increased from 350kg m^{-3} to 450kg m^{-3} to account for this effect (Albert et al.,
275 2004; Libois et al., 2014).
3. *Aggregation scheme*: The formation of a new snow layer requires a minimum amount of snowfall. Due to the low accumulation rate at Dome C, the amount of snowfall needed to form a new layer was decreased from 0.03mm h^{-1} to 0.003mm h^{-1} . In the instance when the snowpack has the maximum number of layers (80) at the time a new snow layer is formed, layers with similar properties will be aggregated, resulting in a smoothed signal. The aggregation scheme
280 was disabled for the top 6 layers to resolve realistic near-surface snow temperature profiles and gradients, required to accurately simulate snow metamorphism.

2.3.3 Model initialisation

The snowpack was initialised with density and optical radius profiles measured in January 2010 at Dome C down to 20m (Champollion et al., 2019), and snow temperature data from a probe installed at Dome C in 2012 with 5 cm resolution near
285 the surface, coarsening with depth down to 12m. ERA5 reanalysis data from Dome C was used to force the model at 3-hourly resolution over the period between ~~1st~~ 1 January 2000 and ~~1st~~ 1 December 2020 (Hersbach et al., 2020). The model requires atmospheric forcings for air temperature, accumulation rate, wind speed and direction, incoming shortwave and longwave radiation, and specific humidity. ERA5 gives a mean annual snowfall rate between 2000 and 2020 of $2.3\text{cm w.eq. a}^{-1}$, and as such, the snowfall rate was multiplied by 1.2 to match the observed mean annual accumulation rate of around $2.8\text{cm w.eq. a}^{-1}$
290 (Frezzotti et al., 2004; Libois et al., 2014). To ensure that at least the top ~~1m~~ 1m consists of accumulated snow, a 100-year spin

up was used by running the forcing file ~~10-ten~~ times between 2000 and 2010, followed by the period from 2000 to 2020. The outputs from 2010 to 2020 were then used for analysis.

2.3.4 Sensitivity tests

The sensitivity of snowpack properties to perturbations in surface forcings are tested by modifying one of three forcing parameters: incoming shortwave radiation, accumulation rate, or 2 m air temperature. The magnitude of the perturbation to each parameter correspond to minimum and maximum values reconstructed over the last 800 ka. We use shortwave radiation as a proxy of insolation and scale the values in proportion to the SSI values. A total of seven simulations are used to perform sensitivity analysis and are outlined in Table 2. The model configuration and initial snow profile were kept constant for each simulation; only the tested parameter in the atmospheric forcing file was modified as follows:

300 ~~Overview of modifications made to forcing test parameter in Crocus snowpack sensitivity test scenarios. Simulation-Reference~~
~~SSI-min SSI-max A-min A-max T-min T-max Incoming-SWR (Scaled)-100% 85% 111% 100%-100%-100%-100%~~
~~Accumulation rate (cm w.eq. a⁻¹)-2.8 2.8 2.8 1.0 4.1 2.8 2.8 Air temperature (°C)-55 -55 -55 -55 -55 -65 -51~~

Summer solstice insolation (SSI): Over the last 1000 years, the average SSI at 75.1°S was 544 W m⁻² (Laskar et al., 2004), compared to 462 W m⁻² and 601 W m⁻², corresponding to minimum and maximum SSI over the past 800 ka. To translate to forcing perturbations, the incoming shortwave radiation (SWR) is scaled by 85% and 111%, respectively to reach the target values (462 W m⁻² and 601 W m⁻²). No additional modifications are applied to annual distribution of SWR.

Annual mean accumulation rate (A): Present-day accumulation rate at Dome C is set to 2.8 cm w.eq. a⁻¹ ~~in the ERA5 forcing following Libois et al. (2014)~~. Hereafter, accumulation rate is expressed as ice equivalent centimetres per year. ERA5 snowfall was scaled by 36% to reach the target accumulation rate of 1.0 cm w.eq. a⁻¹, representing the 800 ka minimum, and 146% to produce an accumulation rate of 4.1 cm w.eq. a⁻¹ which corresponds to the 800 ka maximum (Bazin et al., 2013).

Annual mean air temperature (T): Snowpack sensitivity to air temperature is tested by decreasing the 2 m air temperature by 10°C for glacial conditions (Jouzel et al., 2007), and applying a 4°C, increase to represent 800 ka maximum temperatures. We note, however, that borehole temperature measurements and delta-age are more consistent with a 5°C cooling (Buizert, 2021)(Buizert et al., 2021). Furthermore, these temperature modifications do not include changes in seasonal temperature variability but suffices for the purpose of identifying bulk changes in the snow properties. The average seasonal cycle is kept constant with an average amplitude of 35°C.

It is important to highlight that, at polar sites, accumulation rate is dependent on temperature, and temperature is influenced by insolation, such that these parameters are not independent. However, we use the model to constrain the influences of each forcing parameter in an independent manner to understand the mechanisms, even if, in reality, these parameters are inter-dependent.

Table 2. Overview of modifications made to forcing test parameter in Crocus snowpack sensitivity test scenarios.

Simulation	~	Reference	SSI min	SSI max	A min	A max	T min	T max
Incoming SWR	(Scaled)	100%	85%	111%	100%	100%	100%	100%
Accumulation rate	(cm w.eq. a ⁻¹)	2.8	2.8	2.8	1.0	4.1	2.8	2.8
Air temperature	(°C)	-55	-55	-55	-55	-55	-65	-51

3 Results

3.1 Influence of SSI and local climate on $\delta O_2/N_2$ variability in ice cores

Figure 2 shows $\delta O_2/N_2$ versus SSI for EDC, Dome F and South Pole. These three sites are used owing to their long temporal range and high-resolution $\delta O_2/N_2$ measurements, but with negligible gas loss. The regression slopes vary between $-0.09 \pm 0.006 \text{‰} \cdot \text{m}^2 \cdot \text{W}^{-1} \cdot \text{m}^2$ for South Pole to $-0.06 \pm 0.005 \text{‰} \cdot \text{m}^2 \cdot \text{W}^{-1} \cdot \text{m}^2$ for EDC. The regression for Dome F falls within 2 standard deviations (2σ) of the regression for EDC, but the regression for South Pole falls just outside the 2σ uncertainty. Furthermore, the $\delta O_2/N_2$ is shifted for South Pole compared to EDC, evidenced by the increased y-intercept from -18.9‰ at EDC to 40.6‰ at South Pole. Inter-site differences in the dependence of absolute $\delta O_2/N_2$ on SSI suggest values from South Pole are higher than for EDC and Dome F for the same SSI, suggesting additional factors are influencing the records, such as accumulation rate, which at South Pole is over double around three times that of both EDC and Dome F or integrated summer insolation. In the following sections, we provide evidence for the influences of accumulation rate and air temperature on $\delta O_2/N_2$, in addition to SSI, using both spatial (inter-site) and temporal (EDC ice core) variability of $\delta O_2/N_2$.

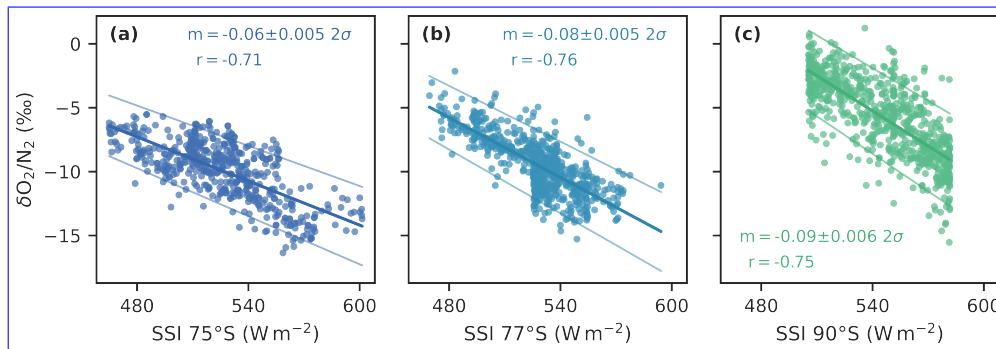


Figure 2. Scatter plots showing the negative correlation between SSI and $\delta O_2/N_2$. Significant negative correlations (over 99% confidence) are observed using relatively high resolution data from Dome C (dark blue; Bouchet et al., 2023a), EDC (Bouchet et al., 2023), (b) Dome F (mid-blue; Kawamura et al. (Kawamura et al., 2007; Oyabu et al., 2021), 2007; Oyabu et al., 2021), and (c) South Pole (green; Severinghaus et al. (Severinghaus, 2019), 2019). The slope (m, units $\text{‰} \cdot \text{m}^2 \cdot \text{W}^{-1} \cdot \text{m}^2$) and r^2 -values are presented for each site.

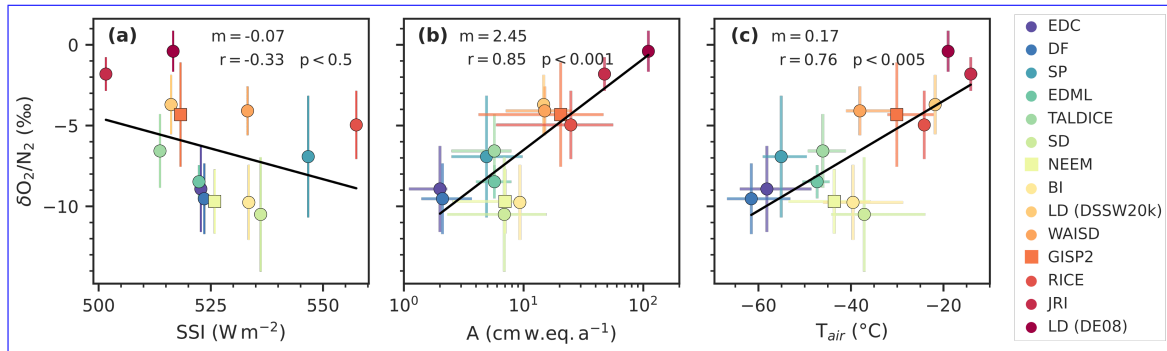


Figure 3. Scatterplots showing the dependence of $\delta\text{O}_2/\text{N}_2$ on a) SSI, b) accumulation rate (A), and c) air temperature (T_{air}). Each point represents the mean values of each site over the depth interval in Table 3. Error bars on y-axis show the standard deviation of $\delta\text{O}_2/\text{N}_2$, while x-axis error bars in (b) and (c) show the range of values over the depth interval. Linear regressions are shown in black, along with the associated slope (m), correlation coefficient (r), and p-value.

3.1.1 Inter-site comparison of mean $\delta\text{O}_2/\text{N}_2$

335 In addition to the $\delta\text{O}_2/\text{N}_2$ datasets, we compile ~~accumulation rate~~ SSI, ~~accumulation rate~~, and temperature reconstructions from each site ~~covering the same depth range as the~~ and take the mean values over the time periods which overlap in all records (Table 3). ~~Drivers of mean $\delta\text{O}_2/\text{N}_2$ data. Due to the inclusion of measurements from varying depths, and thus, ages, between sites, we include the~~ are then explored using regression analysis as presented in Fig. 3. The range of accumulation rates and temperatures ~~over the given time period are included as error bars in Fig. 3b and 3c~~ to indicate the climate histories for each site (Table 3). ~~The data are presented in Figure 3 for a) 1000-year averaged SSI, b) accumulation rate, and c) temperature. Error bars in panel a) and b) indicate the range of values with the exceptions of; Berkner Island and James Ross Island, where the minimum, maximum, and mean accumulation rate and temperature values are approximated as . SSI ranges for each site are excluded given that they are substantially larger than the range in mean SSI between sites. Due to limited data availability from the Berkner Island ice core we take the average temperature and accumulation rate using present day values and last~~ glacial maximum values (Capron et al., 2013), ~~the present day values, and the mean of these two values, respectively; and, Law Dome sites. This is justified given that the data spans approximately the last glacial maximum to the start of the Holocene (Massam, 2018). Finally, present-day values are used for accumulation rate and temperature at DE08 and DSSW20k, where only the present-day values are used. We acknowledge that the former approximation may introduce a bias towards cold, low-accumulation conditions due to the relatively young ages corresponding to the $\delta\text{O}_2/\text{N}_2$ data (~90 a BP).~~

350 ~~As expected,~~

~~No significant correlation is observed between mean $\delta\text{O}_2/\text{N}_2$ is anti-correlated with SSI and SSI in Fig. 3a ($r = -0.47-0.33$, $p < 0.1$) with a 0.5), but the slope of -0.07 , $\% \text{O}_2/\text{N}_2 \text{ W}^{-1} \text{m}^2$ is the same as observed in Figure 2. However, in addition to the influence of SSI, we find a stronger, more Fig. 2. In contrast, Fig. 3b and 3c show a strong, significant correlation between mean $\delta\text{O}_2/\text{N}_2$ and both temperature the natural log of accumulation rate ($r = 0.72-0.85$, $p < 0.001$) and the natural log of accumulation~~

355 ~~rate-temperature~~ ($r=0.81$, $p<0.001$)—the logarithmic dependence suggesting increased sensitivity at low accumulation
~~rates~~ (0.005). The linear model in ~~Figure 2~~ Fig. 3b indicates that a doubling of accumulation rate would result in a ~~1.51~~ 1.3%
increase in $\delta O_2/N_2$ ($\delta O_2/N_2 = 2.2 \cdot \log(A) - 12$ ~~$\delta O_2/N_2 = 2.5 \cdot \log(A) - 12$~~). However, it is important to note that tem-
perature and the logarithm of accumulation rate are strongly correlated in Antarctica, such that the correlations seen in panels
~~(ab) and (b) of Figure c) of Fig. 3~~ are dependent on one another.

360 ~~Large residuals in Figure 2a can partially be attributed to the use of 1000-year average SSI instead of averages over the same~~
~~time periods as the $\delta O_2/N_2$ data. This would require age-scales for all sites.~~ Deviations from the $\delta O_2/N_2$ -SSI regression line
~~may also be attributed~~ regression lines in Fig. 3b and 3c may be linked to discrepancies in site latitude resulting from the ice
flow speed at different sites. Indeed, data from NEEM were measured on ice between 1757 and 2525 m depth (approximately
~~38-130 ka~~ 38–130 ka BP), when the ~~ice-site~~ would have been upstream of the current site at a lower latitude (Rasmussen
365 et al., 2013; Members, 2013). ~~Berkner Island, NEEM~~ In the case of Berkner Island and Siple Dome ~~fall below the regression~~
~~lines in panels b) and c).~~ For Berkner Island, this may be linked to the method used to determine the mean accumulation
rate and temperature values. Other explanations may be linked to procedural artefacts such as, ~~we suggest that relatively low~~
 ~~$\delta O_2/N_2$ values are the result of storage gas loss effects (Section 2.2.3) given that the measurements were carried out ~ 7 and~~
 ~~~ 8 years after coring for Berkner Island and Siple Dome, respectively. While clathrates are reportedly absent from both sites~~
370 ~~(Mulvaney et al., 2007; Neff, 2014), the low values may link to gas loss during storage within increasingly brittle ice at depth~~
~~in the core.~~

Scatterplots showing the dependence of $\delta O_2/N_2$ on the a) SSI, b) accumulation rate (A), and c) annual average temperature
(T_{air}). Each point represents the mean values for each site over the depth interval of included $\delta O_2/N_2$ data for each site (Table
3). Error bars represent the range of values over the depth interval. Error bars on y-axis show the standard deviation of $\delta O_2/N_2$
375 measurements, and the x-axis in b) and c) show the range in accumulation rate and temperature. In each panel, the black
line shows the linear regression between $\delta O_2/N_2$ and each parameter, along with the associated correlation coefficient (r) and
p-value. Data shown here are presented in Table 3, while information on the individual datasets can be found in Table S1 and
S2 in the supplement. *Present-day accumulation rate and temperature have been used for the two Law Dome sites; DE08 and
DSSW20k.

380 3.1.2 Temporal variability of $\delta O_2/N_2$ at Dome C

High resolution data is required to investigate the temporal variability in $\delta O_2/N_2$ as a function of accumulation rate, ~~temperature,~~
~~and SSI~~ and temperature. The δ -deuterium (δD) record from water isotope measurements is used as a qualitative proxy for ac-
cumulation rate and temperature, whereby higher δD values are generally associated with increased accumulation rate and
temperature in ice cores from the East Antarctic plateau (Jouzel et al., 2007; Parrenin et al., 2007). The following analysis
385 uses ~~high-resolution~~ the longest period of relatively high-resolution $\delta O_2/N_2$ and δD measurements from the EPICA Dome
C (EDC) ice core (Jouzel et al., 2007; Bouchet et al., 2023), both on the AICC2012 EDC ice core between 190–259 ka BP
(1980–2350 m) on the AICC2023 ice-age scale (Bazin et al., 2013). ~~chronology~~ (Bouchet et al., 2023).

Table 3. Information on ~~An overview of data used in Fig. 3. The depth range of data included may differ from the entire available $\delta\text{O}_2/\text{N}_2$ datasets from~~ ~~between each site after removing measurements influenced by gas loss parameter. Presented Mean values are ; the presented for $\delta\text{O}_2/\text{N}_2$ mean (μ), standard~~ ~~depths (N); the depth range of $\delta\text{O}_2/\text{N}_2$ measurements; the mean (μ), minimum (min) and maximum (max) annual accumulation rate (A), and the annual~~ ~~temperature (T) over SSI at the same depth range as current site latitude. Where age scales are available, the $\delta\text{O}_2/\text{N}_2$ data; and SSI represents the mean~~ ~~been rounded~~ ~~For sites without age scales, the average SSI over last 1000 years is used.~~

height	Site	Site	Depth range	Depth (m)	Age range	$\delta\text{O}_2/\text{N}_2^a$	Accu. rate ^b
~			μ (m)	σ (ka BP)	σ (ka BP)	N (‰)	(cm w. eq a ⁻¹)
	*BIBI ¹		-9.81-609-694		2.8	64-609-694-8.6-9.8 ± 2.3	14.9-9.3
	DFDF ²		-9.76-113-794, 1456-2149	2.5-2.9-38.1, 10.0-207.8		913-9.5 ± 2.2	113-449, 1410-2500-2.1
	EDCEDC ³		-8.91-1421-3189	2.7-105.9-805.1		823-8.9 ± 2.8	1421-3189-2.0
	EDMLEDMI ⁴		-8.5-595-860	1.3-9.3-16.4		5-8.5 ± 1.0	596-860-5.7
	GISP2GISP2 ⁵		-5.84-73-2395	3.7-0.2-50		182-4.3 ± 3.2	73-648, 1515-2428-20.4
	*JRJRI ⁶		-3.13-76-359	2.9-0.03-14.3		16-1.8 ± 1.0	52-364-47.4
	**DE08LD (DE08) ⁷		-1.21-175-218	1.9-0.008-0.011		8-0.4 ± 1.3	175-218-110.3
	**DSSW20kLD (DSSW20k) ⁸		-4.06-61-63	1.6		4-3.7 ± 1.8	61-63-14.7
	NEEMNEEM ⁹		-9.74-1757-2396	2.1-38.1-121.4		119-9.7 ± 2.0	1757-2525-7.0
	RICERICE ¹⁰		-4.98-60-344	0.1-2.6		5-5.0 ± 2.1	387-24.8
	SDSD ¹¹		-9.53-500-969	2.5-7.6-95.0		68-10.5 ± 3.5	69-400-6.9
	SPSP ¹²		-7.87-125-1749	3-1.1-54.2		691-6.9 ± 3.8	125-617, 1078-1751-4.9
	TALDICE TALDICE ¹³		-5.38-155-1072	2.5-1.5-40.0		68-6.6 ± 2.3	155-669, 1003-1402-5.7
	WAISDWAIS ¹⁴		-4.14-80-962, 1700-3397	1.9-0.2-4.1, 9.0-66.2		433-4.1 ± 1.5	80-648, 1602-3397-15.0

References for $\delta\text{O}_2/\text{N}_2$ data, accumulation rate, and temperature correspond to a, b, and c, respectively. ¹This study^a, Capron et al., 2013^{b,c};

²Kawamura et al., 2007^a, Oyabu et al., 2021^a, Watanabe et al., 1999^a, Kawamura et al., 2017^b, Uemura et al., 2018^c;

³Bouchet et al., 2023^a, Extier et al., 2018^a, Bazin et al., 2013^b, Jouzel et al., 2007^c;

⁴This study^a, Bazin et al., 2013^b, Stenni et al., 2010^c;

⁵This study^a, Suwa and Bender, 2008b^a, Cuffey and Clow, 1999^b, Clow, 1999^c;

⁶This study^a, Capron et al., 2013^b, Mulvaney et al., 2012^{b,c};

⁷Buizert et al., 2020^a; Rubino et al., 2013^b, Etheridge and Wookey, 1988^c;

⁸Buizert et al., 2020^a, Rubino et al., 2013^b, Morgan et al., 1997^c;

⁹This study^a, Rasmussen et al. (2013)^a, Rasmussen et al., 2013^{b,c};

¹⁰Lee et al., 2020^a, Winstrup et al., 2019^b, Bertler et al., 2017^c;

¹¹Severinghaus, 2009^a, Buizert, 2021^{b,c};

¹²Severinghaus, 2019^a, Kahle et al., 2020^{b,c};

¹³This study^a, Bazin et al., 2013^{b,c};

¹⁴Severinghaus, 2015^a, Fudge et al., 2017^b, White et al., 2019^c. *JRI and BI using LGM and present-day values (Capron et al., 2013) as the maximum and minimum values for Dome sites.

Two approaches are used to extract the non-SSI signals in the $\delta\text{O}_2/\text{N}_2$ records used for orbital dating require the filtering of noise and. First, we interpolate SSI onto the $\delta\text{O}_2/\text{N}_2$ ages and take the deviations from the $\delta\text{O}_2/\text{N}_2$ -SSI linear regression to isolate the $\delta\text{O}_2/\text{N}_2$ variability not explained by SSI (hereafter, $\delta\text{O}_2/\text{N}_2$ -SSI residual). The second approach directly investigates the millennial-scale variability (Kawamura et al., 2007; Landais et al., 2012). However, no filtering is applied here in order to resolve variability over shorter timescales. The new measurements cover five distinct sections of the core between 111 and 539 ka BP (Bouchet et al., 2023). We primarily focus on the longest section between 180-259 ka BP (1980-2350m) which covers MIS-7 variability by applying a low pass filter to the $\delta\text{O}_2/\text{N}_2$ and δD records (interpolated onto a 100-year time step), using a 10-kyr cut-off to isolate the low-frequency signals associated with SSI. The filtered curves are then subtracted from the original curves to remove the orbital (SSI) signal, and a 5-point moving average is applied to the residuals to reduce noise but retain millennial-scale variability in the records.

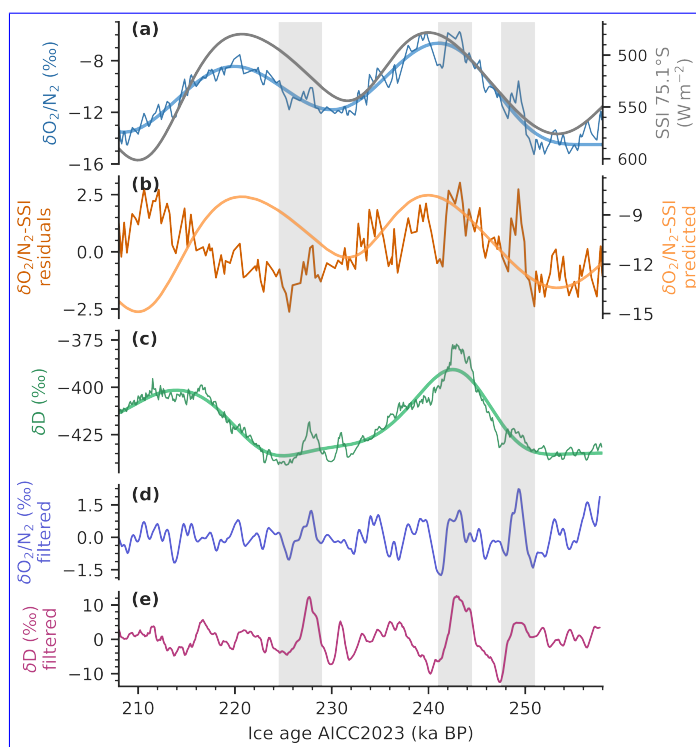


Figure 4. Evolution of $\delta\text{O}_2/\text{N}_2$, SSI and δD on the AICC2023 ice age timescale from EDC (Bouchet et al., 2023). Panel (a) presents the 100-year interpolated $\delta\text{O}_2/\text{N}_2$ overlain with the low pass filtered curve (blue). The right y-axis in panel (a) shown SSI at 75.1°S (grey). The predicted $\delta\text{O}_2/\text{N}_2$ as a function of SSI ($\delta\text{O}_2/\text{N}_2$ -SSI predicted) is shown on the right axis of panel (b), and the residuals of the observed $\delta\text{O}_2/\text{N}_2$ and predicted are on the left axis. Panel (c) shows the 100-year interpolated δD overlain with the low pass filtered curve (green). The bottom two panels present the residuals of the low pass filtered curves for $\delta\text{O}_2/\text{N}_2$ (d) and δD (e). Grey bars highlight the pronounced millennial-scale variability.

In Figure 4, the Figure 4 primarily shows the dominant SSI cyclicity in the $\delta O_2/N_2$ curve is dominated by the SSI cyclicity record, as has been documented previously (e.g., Landais et al., 2012). Superimposed onto this signal are millennial-scale peaks in $\delta O_2/N_2$ which appear to coincide with peaks in δD , highlighted by grey bars in Figure 4e. To evaluate additional climatic signals in the EDC $\delta O_2/N_2$ records, we first remove the SSI signal from the record using the residuals of the linear regression between $\delta O_2/N_2$ and SSI (Figure 2b). We observe that, in addition to the This high frequency variability is more clearly identified from the filtered curves in Fig. 4d and 4e. The coherence between millennial-scale variability, some long-term variability remains which would not be expected if peaks in $\delta O_2/N_2$ was controlled by SSI alone. Indeed, there is a stronger significant positive correlation between δD and SSI- $\delta O_2/N_2$ residuals on the ice-age scale between 190-260 ka BP (Figure 4d; $r=0.68$, $p<0.001$), than δD and $\delta O_2/N_2$ (Figure 4e; $r=0.43$, $p<0.001$). This D suggests a positive correlation with accumulation rate and temperature and, which shares analogy with the spatial positive correlation between $\delta O_2/N_2$ and both accumulation rate and temperature (Figure Fig. 3). Applying the same analysis to the other periods of high-resolution measurements results in significant positive correlations for all but the period between 409 and 449 ka BP (Figure S3 in Supplement). We note a remnant 20-kyr variability in the $\delta O_2/N_2$ -SSI residual which is in phase with δD . This orbital-scale signal is present when using either the AICC2012 chronology or the AICC2023 chronology (Bazin et al., 2013; Bouchet et al., 2023). Given that the new AICC2023 age scale (used here) has been orbitally tuned using this data (Bouchet et al., 2023), this signal is not expected to be the result of phase difference between the EDC chronology and SSI.

Evolution of $\delta O_2/N_2$, SSI and δD on the AICC2012 ice age timescale from Dome C (Bazin et al., 2016; Bouchet et al., 2023) - Panel a) presents the $\delta O_2/N_2$ (blue) with SSI on the right y-axis (grey), b) the $\delta O_2/N_2$ -SSI residuals (orange), and c) δD (green), over the period between 210 and 260 ka BP. Correlations between δD and $\delta O_2/N_2$, and between δD and the $\delta O_2/N_2$ -SSI residuals are presented in d) and e), respectively.

3.2 Crocus model results

3.2.1 Crocus model evaluation for Dome C

The Crocus model outputs are first evaluated by comparing the reference simulation (Ref in Table 2) to observational data from Dome C. Simulated density and SSA profiles are compared to data from Libois et al. (2014), measured daily between 23rd November 2012 and 16th January 2013 at two sites within 600m of Concordia station, Dome C. Density was measured at 2.5cm resolution down to 25cm, while SSA was measured at 1cm depth intervals down to 50cm. Snow temperature at Dome C has been continuously measured since 2012 at 30-minute intervals. Simulated snow density and SSA were interpolated to a fixed grid of 1cm depth resolution and a 24-hour timestep between 2010-01-01 and 2020-12-01 1 January 2010 and 1 December 2020, while snow temperature was interpolated onto a 1mm by 6-hourly grid over the same time period.

Density and SSA outputs presented in Figure Fig. 5a and 5b are averaged values over the measurement period (23rd November 2012 and 16th January 2013). For the most part, the observations fall within the range of the simulations. Density is well-simulated throughout the top 25cm. The simulated SSA profile is consistently within one standard deviation of the measurements below 10cm, above this depth, simulated SSA is overestimated by up to $10\text{m}^2\text{kg}^{-1}$. In contrast, density is

~~well-simulated throughout the top 25 cm.~~ Small standard deviations associated with simulated density and SSA, suggests that variability is not well reproduced. As discussed in Libois et al. (2014), the standard version of Crocus is unable to reproduce density and SSA variability with depth due to its one-dimensional nature. For the purpose of our study, we consider the standard version sufficient to assess the overall sensitivity of snowpack properties to perturbations in forcings.

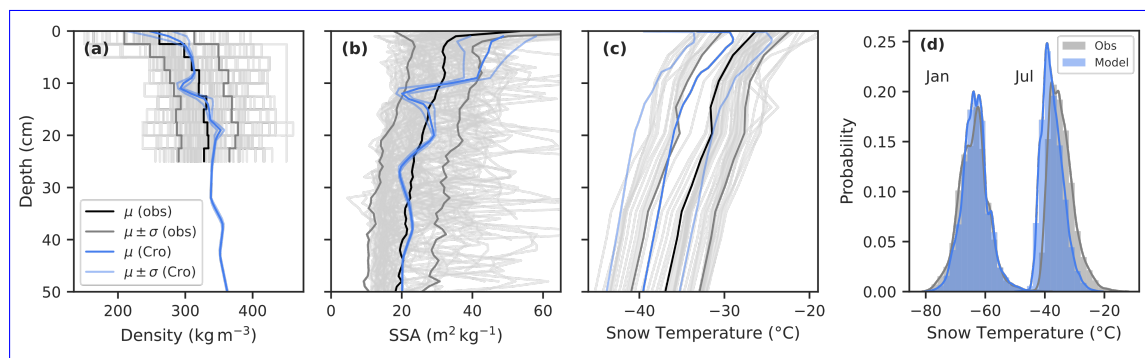


Figure 5. Comparison of observations and Crocus simulated snowpack profiles. Density (a) and SSA (b) profiles represent the average from 23 November 2012 and 16 January 2013, to cover the measurement period (Libois et al., 2014). The snow temperature (c) profiles both from Crocus and the observations are the average from 23 November 2019 and 16 January 2020. Faded grey lines represent individual profiles from observations, and the shaded bands show the standard deviations. Snow temperature distributions (d) from January and July between 2016 and 2020.

435 Snow temperature in ~~Figure Fig.~~ 5c covers the period between 23 ~~rd~~ November 2019 and 16 ~~th~~ January 2020. A 3°C cold bias is apparent, but the mean falls within 1σ of the observations. Figure 5d presents distributions of the stacked January snow temperatures between 2016 and 2020, further showing this 3°C cold bias during summer ($-37.1 \pm 3.6^\circ\text{C}$ and $-34.4 \pm 4.1^\circ\text{C}$ for Crocus outputs and observations, respectively). However, ~~stacked July winter~~ snow temperatures are well simulated with a 1 m mean of $-64.7 \pm 4.5^\circ\text{C}$ and $-63.9 \pm 5^\circ\text{C}$ from Crocus outputs and observations, respectively. The overestimation of ~~simulated~~ SSA in the top 10cm may be linked to the ~~summer cold bias in near-surface snow temperature, reducing the modelled snow temperature during summer via the reduced~~ rate of snow metamorphism in near-surface ~~grains snow~~. Alternatively, high SSA may be the result of a recent precipitation event. During large precipitation events the fresh snow will be buried rapidly and undergo less metamorphism than the topmost snow given that most metamorphism occurs in the top 5 cm where solar radiation drives strong temperature gradients (Picard et al., 2012). This could result in sustained high SSA in the top 10cm.

445 ~~Comparison of observations and Crocus simulated snowpack profiles. SSA (a) and density (b) profiles represent the average from 23rd November 2012 and 16th January 2013, to cover the measurement period (Libois et al., 2014). The snow temperature (c) profiles both from Crocus and the observations are the average from 23rd November 2019 and 16th January 2020. Faded grey lines represent individual profiles from observations, and the shaded bands show the standard deviations. Snow temperature distributions (d) from January and July between 2016 and 2020.~~

450 3.2.2 Simulated response of snowpack properties to surface perturbations

Sensitivity tests were run using the Crocus model to assess the response of near-surface snowpack properties to perturbations in local surface forcings. The following analysis uses optical radius as a measure of grain size – which is directly linked to SSA and the density of ice (Section 2.3.1) – and focuses on the response of near-surface snow density and grain size to the six scenarios outlined in Table 2. We firstly assess the bulk changes in physical properties before looking at the variability with
455 depth.

3.2.3 Bulk snowpack sensitivity

Numerous studies have suggested that modifications in near-surface density and grain size are key parameters influencing elemental fractionation during pore closure (e.g., [Bender, 2002; Fujita et al., 2009](#); [Bender, 2002; Fujita et al., 2009](#)). Figure 6c and 6d show shows the mean difference in density and grain size from the Dome C reference simulation (Ref) and each of the
460 test scenarios (outlined in Table 2). Overall, grain size is more sensitive to changes in surface forcing than density in the upper 20 cm. The sensitivity tests reveal that a 15% decrease in SSI (SSI min) decreases grain size by 8% and an 11% increase in SSI (SSI max) causes a 12% increase in grain size. Both directions of perturbation result in <1% change in density. The magnitudes of change in both density and grain size are much larger under accumulation rate and temperature perturbations than under SSI perturbations.

465 Accumulation rate and temperature have the opposite effect on density and grain size. A 4°C increase in temperature (T max) increases density and grain size by 8% and 29%, respectively, while an increasing the accumulation rate to 4.1 cm w.eq. a⁻¹ (A max) results in a 7% decrease in density and a 10% decrease in grain size. ~~These opposing influences~~ The opposing influence of accumulation rate and temperature ~~on snow properties~~ at first appears to contradict the observations in [Figure 3](#), ~~whereby Fig. 3, where~~ $\delta\text{O}_2/\text{N}_2$ increases with both ~~accumulation rate and temperature. This can be attributed to co-linearity~~
470 ~~between accumulation rate and temperature. We also note the non-linear response of variables.~~ Mean density and grain size respond non-linearly to perturbations in all ~~forcings – most evident is the sensitivity of grain size to accumulation rate.~~ forcing parameters, as is shown by the magnitude of increase in grain size from decreased accumulation rate being three times greater than the magnitude of decrease induced by an increase in accumulation rate (right panel of Fig. 6c, green bars). This is in line with the dependence of $\delta\text{O}_2/\text{N}_2$ to the logarithm of accumulation rate documented in [Figure Fig. 3](#).

475 3.2.4 Depth variability sensitivity

An alternative (although possibly ~~complimentary~~ complementary) explanation for the mechanistic control of snow properties on elemental fractionation links to stratigraphic layering due to seasonality (Fujita et al., 2009). Here we explore the influence of layering by looking at the depth variability in density and grain size as a qualitative measure of stratification (Hörhold et al., 2011), assuming that higher variability indicates stronger layering. Variability is defined as the standard deviation of each depth
480 interval (denoted σ) over the period between January ~~1st~~ 1st 2010 and December ~~1st~~ 1st 2020.

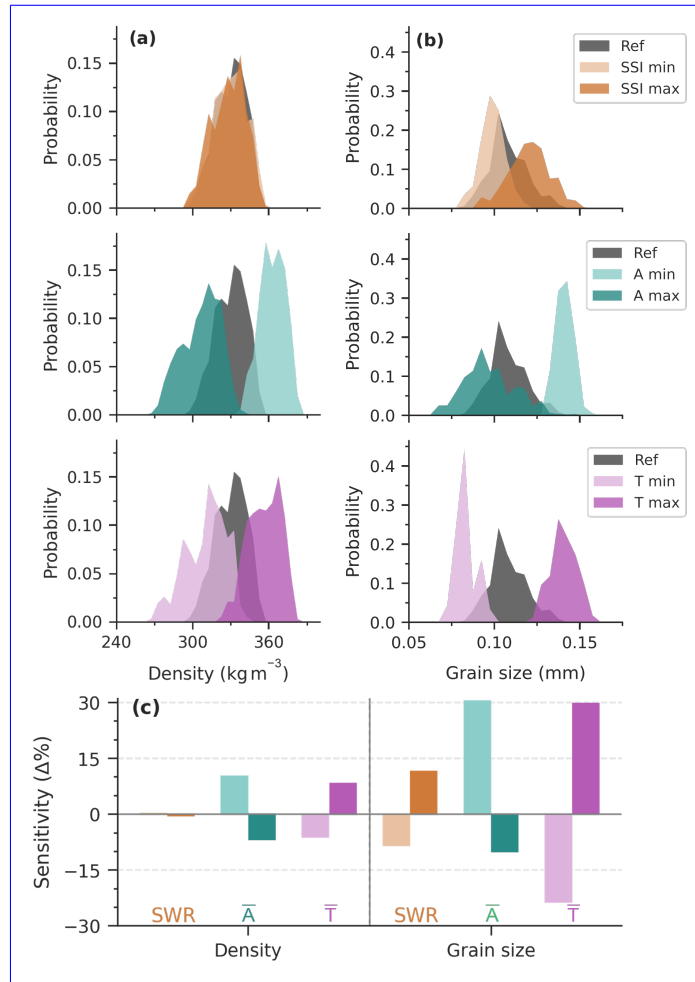


Figure 6. Comparison of density and grain size (r_{opt}) over the top 20cm from Crocus sensitivity simulations. Distributions of a) density and b) grain size outputs from each test simulation are compared to the reference simulation (bin size is 5 kg m^{-3} , and 0.005 mm). In panel c) bars represent the percentage change in mean density and mean grain size for perturbations in SSI (orange), accumulation rate (green), and temperature (purple); with the decreased scenarios represented by the faded colour, and the increased by the bold colour.

The σ values for each simulation are presented in Figure Fig. 7 for the top 1 m of snowpack. In all runs, σ peaks near the surface and decreases with depth for both density and grain size (σ_ρ and σ_{g_s}). Density variability for four out of the six test simulations is largely similar to the reference. High-accumulation rate (A max) and low-temperature (T min) are the exception, with an increase in σ_ρ of up to 5 kg m^{-3} compared to all other runs. Surprisingly, the increased σ_ρ values correspond to a decrease in mean density in the A max and T min simulations (Figure Fig. 6). The spread in σ_{g_s} between simulations is broader than for σ_ρ over the top 50cm, with T min, SSI min, A min, and T max all resulting in reduced variability compared to the reference run. σ_{g_s} appears to increase with an increase in SSI and accumulation rate throughout the top metre.

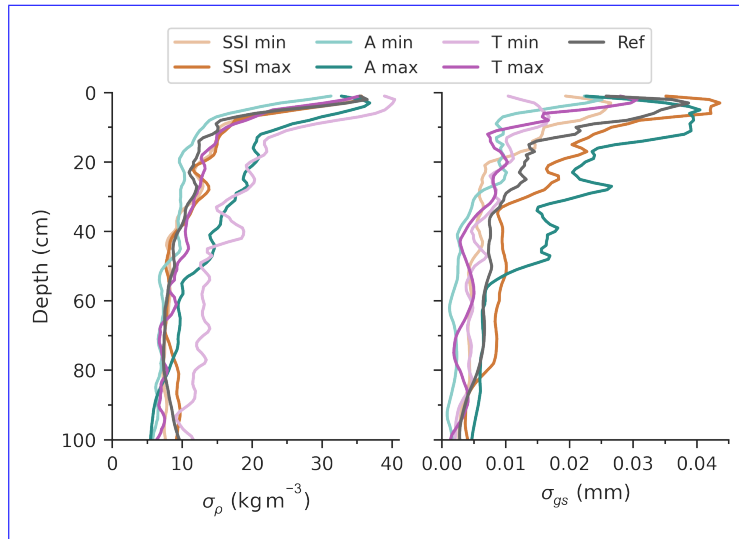


Figure 7. Variability in density and grain size with depth over the top 1 m. Each pair of simulations is represented by a colour, SSI in orange, accumulation rate in green, and temperature in purple. The faded line of each pair represents the 800-ka minimum simulation, and the bold line represents the 800-ka maximum simulation.

To summarise, outputs from the Crocus model indicate that insolation modifies mean grain size but has negligible effect on mean density in the top 20 cm. On the other hand, higher air temperature and lower accumulation rate result in increases in both mean density and mean grain size, although this change is not necessarily proportional. The depth variability of the two snowpack parameters is strongly influenced by increased accumulation rate, with decreased temperature also having a large effect on density variability, and increased SSI causing an increase in grain size variability. At 100 cm, there is no significant difference in the σ_ρ and σ_{gs} for the different forcing scenarios, which is discussed in Section 4.3.2.4.4.

4 Discussion

4.1 Evidence for non-SSI dependence of $\delta O_2/N_2$

Our compilation of different deep ice core $\delta O_2/N_2$ records show in Fig. 2 reinforces the widely documented anti-correlation between SSI and $\delta O_2/N_2$ on the ice-age scale (Kawamura et al., 2007; Landais et al., 2012; Suwa and Bender, 2008a; Oyabu et al., 2022; Bouchet et al., 2023). However, a comparison of EDC, Dome F, and South Pole (as the only 3 cores with sufficient long and high resolution $\delta O_2/N_2$ records not affected by gas loss for this study) reveals an additional latitudinal dependence of the slope of the linear regression, whereby the highest latitudes have the steepest slope (SP 90°S = -0.09% \cdot m²·W⁻¹, DF 79°S = -0.06% \cdot m²·W⁻¹, EDC 75°S = -0.05% \cdot m²·W⁻¹; Figure 2). This suggests Fig. 2) reveals an additional influence of site conditions such as integrated summer insolation (ISI) (Huybers and Denton, 2008), which is not surprising given the mechanistic overlap with total air content (TAC) variability (Fujita et al., 2009). Inter-site analysis reveals a dependence of

mean $\delta O_2/N_2$ on SSI (average over the last 1000 years) with both temporal (Figure 2) and spatial (Figure 3e) data falling on the same regression slope ($\delta O_2/N_2$ is strongly correlated with accumulation rate and temperature (Fig. 3). Interestingly, SSI does not significantly influence site mean $\delta O_2/N_2$ ($-0.07\% \cdot m^2 \cdot W^{-1}$). We also observe new evidence that mean $\delta O_2/N_2$ is significantly dependent on local temperature and accumulation rate, most apparent in the dependence of mean $\delta O_2/N_2$ on the natural log of accumulation rate (Figure 3b). may link to the range of variations in the three forcing parameters. For example, the spatial variations in accumulation rate are much larger than the variations at a single site through time. Conversely, the spatial range of SSI values is between $500\text{--}560 \text{ W m}^{-2}$, whereas the range at EDC, for example, is between $470\text{--}600 \text{ W m}^{-2}$. Further investigation into

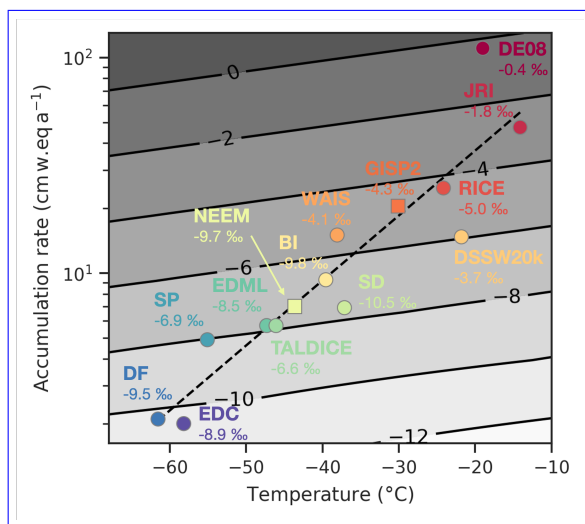


Figure 8. $\delta O_2/N_2$ as a function of accumulation rate and temperature ($Avg. \delta O_2/N_2 = 0.03 \cdot T + 2.8 \cdot \log(A) - 14.3$). Measured mean $\delta O_2/N_2$ values are noted alongside each site. The accumulation rate-temperature regression (dashed, black line) is defined using a regression on temperature and accumulation rate for all sites in the data compilation.

To further constrain the drivers of $\delta O_2/N_2$ variability at Dome C revealed a significant dependence on, we construct a multiple regression to parameterize mean δD (a proxy for O_2/N_2 as a function of accumulation rate and temperature on the long-time scale considered here). Between 190 and 260 ka BP at Dome C, the residuals of the (Fig. 8). Combined, accumulation rate and temperature can explain up to 70% of the total variance in mean $\delta O_2/N_2$ -SSI regression are strongly correlated with. Adding SSI does not improve the adjusted r^2 of the multiple regression. Results are summarised in Fig. 8 and reiterate that δD ($r=0.62$, $p<0.001$), both on the AICC2012 ice-age scale. This relationship is maintained in four out of five sections of high-resolution measurements from the EDC core (Figure S3), with the age range of the outlying section (409–449 ka BP) coinciding with onset of MIS 11 (424–374 ka BP).

The temporal analysis from Dome C initially contradicts the findings from Kobashi et al. (2015), who show an anti-correlation between accumulation rate and $\delta\text{ArO}_2/\text{N}_2$ (and thus, is highly sensitive to accumulation rate, especially at low accumulation sites. The site dependence of $\delta\text{O}_2/\text{N}_2$) at GISP2, Greenland. However, this anti-correlation is observed when we observe has been noted in previous studies. Indeed, Bazin et al. (2016) identified an offset in absolute $\delta\text{ArO}_2/\text{N}_2$ is drawn on a gas-age scale while our observations are performed on values in the Vostok core compared to Dome F and EDC, similar to our observation in Fig. 2. By including records from numerous ice cores we are able to definitively show that absolute values are systematically linked to site accumulation rate and temperature.

4.2 Millennial scale variability in $\delta\text{O}_2/\text{N}_2$ records

Further investigation into drivers of $\delta\text{O}_2/\text{N}_2$ drawn on the ice-age scale. Moreover, (Suwa and Bender, 2008b) found a positive correlation between variability in the EDC core reveals a millennial-scale climate signal in the $\delta\text{O}_2/\text{N}_2$ variability and local temperature at GISP2. This apparent contrast in the link between records. The timing of these anomalies in $\delta\text{O}_2/\text{N}_2$ (or correspond to those in the $\delta\text{Ar}/\text{N}_2$) and accumulation rate variability is also reflected in TAC records. Superimposed to orbital variations driven by ISI (Lipenkov et al., 2011), TAC also exhibits shorter, D record from EDC between 200–260 ka BP (Fig. 4). This suggests that millennial-scale variations which are correlated with accumulation rate at SP, Antarctica (Epifanio et al., 2023) but anti-correlated at NGRIP, Greenland (Eicher et al., 2016) — all considered on the gas-age scale. The observations from Kobashi et al. (2015) and Eicher et al. (2016) suggest additional mechanisms may be at play at high accumulation sites in Greenland, which are evident in the can arise from changes in accumulation rate and/or temperature. The anomalies observed in the EDC $\delta\text{O}_2/\text{N}_2$ and TAC records over millennial timescales. Our overarching aim is to improve the use of record are not unique to this period but vary between time periods and sites (Supplement S2). Indeed, a similar effect was previously observed in the GISP2 core, where $\delta\text{O}_2/\text{N}_2$ as a dating tool, and therefore, we focus on the mechanisms controlling was found to be positively correlated with local temperature over millennial timescales (Dansgaard-Oeschger events) (Suwa and Bender, 2008b)

Previous studies suggest an overlap between the drivers of $\delta\text{O}_2/\text{N}_2$ variability at Antarctica sites — or rather, low accumulation sites — where accumulation increase leads to an increase in and those of total air content (TAC) variability (Fujita et al., 2009; Lipenkov et al., 2011). Ice core $\delta\text{O}_2/\text{N}_2$ —

4.3 Proposed mechanisms controlling $\delta\text{O}_2/\text{N}_2$ variability

Several mechanisms have been proposed to explain variations in and TAC records exhibit slight differences in their spectral signals, whereby $\delta\text{O}_2/\text{N}_2$ and TAC and could be considered in light of our new findings; namely, 1) the effect of residence time in the LIZ, specifically referring to the time taken for pores to close-off (Severinghaus and Battle, 2006; Lipenkov et al., 2011); 2) transient effects from rapid climatic changes driving variations in overburden pressure on the closing bubbles (Kobashi et al., 2015; Eicher et al., 2016); and 3) effects in dominated by precession (hence SSI pacing), whereas TAC is dominated by obliquity (hence the integrated summer insolation pacing). However, variability in both records is linked to local insolation via the modulation of near-surface

snow properties and layering which persist throughout the firm (Bender, 2002; Fujita et al., 2009; Severinghaus and Battle, 2006; Gregory et

555 -

1) Severinghaus and Battle (2006) stated that at low accumulation sites, pores will close-off deeper and take longer to fully close, thus, experiencing more total gas loss and, presumably, more elemental fractionation. Moreover, low accumulation sites are usually characterised by a thin lock-in zone which facilitates diffusivity and fugitive gas loss, as is evidenced by young gas ages in deep firm open porosity (Landais, 2004; Witrant et al., 2012). It is plausible that this 'residence time' effect could partially explain our observations of a positive correlation between accumulation rate and, which ultimately influence pore closure processes (Lipenkov et al., 2011). Fujita et al. (2009) hypothesised that the permeation mechanism, driving fractionation of $\delta O_2/N_2$. However, we would expect this signal to be imprinted on the gas age scale — or more likely, an integrated signal over the entire firm column — and as such, this effect alone cannot account for the much stronger correlation between accumulation rate/temperature and, can explain half the variation in TAC, with the rest being driven by effusion. Therefore, we draw on TAC studies to help interpret millennial-scale variability in $\delta O_2/N_2$ on the ice age scale at Dome C. Recent observations found a hemispheric contradiction in the millennial-scale drivers of TAC variability. TAC is anti-correlated with accumulation rate in the NGRIP core (Eicher et al., 2016) but positively correlated in the South Pole ice core (Epifanio et al., 2023).

2) Short-term (Several mechanisms have been proposed to explain millennial-scale) variations of variability in TAC and $\delta O_2/N_2$. Eicher et al. (2016) attributed the anti-correlation between TAC and accumulation rate during Dansgaard-Oeschger ($\delta Ar/N_2$) and TAC with accumulation rate have been linked D-O events at NGRIP to transient effects in the firm column, resulting from rapid climatic changes (Kobashi et al., 2015; Eicher et al., 2016). During the initial stage of a Dansgaard-Oeschger the D-O event, rapid increases in accumulation rate cause overburden pressure to increase, while more time is needed for the firm column temperature to respond (Eicher et al., 2016). Eicher et al. (2016) suggest that these transient effects explain the increase overburden pressure, reducing the pore volume at close off, and hence, TAC (Eicher et al., 2016). Changes in overburden pressure were also proposed to explain an anti-correlation observed between accumulation rate and TAC on the gas age scale at high-accumulation sites. On the other hand, Kobashi et al. (2015) propose an alternative microbubble mechanism to explain the between $\delta Ar/N_2$ response to rapid climatic change. Such effects are expected to be negligible at low-accumulation sites such as Dome C where accumulation variations are gradual. Moreover, the associated direction of change in (and thus, $\delta O_2/N_2$ during high accumulation conditions is opposite to our observations, potentially indicating that the dominant mechanisms vary between low- and high-accumulation sites, as suggested by Epifanio et al. (2023) with regard to TAC.

3) Near-surface snow properties and layer stratification have been invoked to modulate), and accumulation rate over multi-decadal timescales at GISP2 (Kobashi et al., 2015). In contrast, the positive correlation between TAC and accumulation rate at South Pole is attributed to increased snow burial rates, leading to smaller grains and thus, increased pore volume at close-off (Epifanio et al., 2023). Such a grain size mechanism is understood to drive the integrated summer insolation signal in TAC records (Raynaud et al., 2007), and also the SSI signal in $\delta O_2/N_2$ variability since the first study of Bender (2002). The signal of near-surface snow metamorphism — imprinted in the grain properties — is generally understood to persist throughout

the densification process to the close-off depth, influencing pore closure processes (Bender, 2002). Kawamura et al. (2007) also suggested a link between the strength of metamorphism at the surface and the existence of the lock-in zone leading to records (e.g. Bender, 2002).

Transient effects in the firn column in response to rapid climatic changes (linked to overburden pressure) are expected to be largely absent from Antarctic sites due to reduced magnitude in climate variability compared to Greenland. However, an accumulation-dependent grain size mechanism may explain the positive correlation between δD and $\delta O_2/N_2$ fractionation. In parallel, Raynaud et al. (2007) at EDC. Epifanio et al. (2023) proposed that the metamorphism induced by stronger insolation accelerates grain growth at the surface which later controls porosity in the lock-in zone. Fujita et al. (2009) were the first to focus explicitly on the physical mechanisms governing both elemental fractionation during pore closure and total air content. They provided microstructural data — such as grain size, anisotropy, and a qualitative measure of permeability — from a Dome Fuji firn core and suggested a link between SSI and deep firn density stratification and permeability. They proposed that gas transport via permeation would be more efficient when there is a strong density stratification; such that, increased SSI leads to bulk ice with lower contradictory behaviour of TAC between NGRIP and South Pole may be explained by varying responses of the firn to changes in accumulation rate depending site surface climate conditions. They suggest that a grain size mechanism dominates TAC modulation at low accumulation sites while transient effects from rapid climatic changes are more important at warm, high accumulation sites. We expect that the mechanisms driving $\delta O_2/N_2$ — which agrees with what we observe. However, these studies do not explicitly explore the link between local climate (accumulation rate and temperature) and are also modulated by accumulation rate. Indeed, observations of $\delta O_2/N_2$ variability records from South Pole appear to support the in-phase coherence between $\delta O_2/N_2$ and δD in the EDC core, but only when δD is sufficiently low (Fig. S5 in Supplement). A shifted, anti-phase relationship is apparent when δD is higher, which suggests that different mechanisms may be dominant under high accumulation conditions.

610 4.3 Towards a mechanistic understanding of $\delta O_2/N_2$ variability at low-accumulation sites

While a link between climate and snow metamorphism has been evidenced in previous studies - whereby snow metamorphism is enhanced during summers with very low accumulation rates (Picard et al., 2012; Casado et al., 2021) – the link to pore closure processes has received less attention. Our analysis aims to A possible reason for this is the added complexity which would be required to implement surface snow metamorphism into firn models, accompanied with the need for prior information such as surface grain size. The following sections propose some ideas to bridge this gap by focusing on both local climate parameters and SSI, their influence on near-surface snow metamorphism, and how this might modulate elemental fractionation during pore closure. Crocus snowpack sensitivity tests were used in this study as a first step towards understanding a mechanistic link between physical properties and

4.3.1 Surface snow properties

620 Variations in grain properties are thought to drive the SSI signal in $\delta O_2/N_2$ variability. Our findings support a density-dependent grain size mechanism linking snow metamorphism and elemental fractionation at close-off. Indeed, Calonne et al. (2022)

showed that grain size has a strong influence on permeability, such that for a given density, permeability is increased with grain size. Moreover, Gregory et al. (2014) found that permeability is increased in high-density records (Raynaud et al., 2007). Indeed, large-grain size firn due to a less complex pore structure. The following sections utilise the qualitative differences in bulk snow properties and stratification obtained from the Crocus sensitivity tests to develop a mechanistic explanation for the role of snow properties on pore closure fractionation.

4.3.2 The role of bulk snow properties

SSI sensitivity tests (S_{min} and S_{max} in Table 2) results from sensitivity tests in Fig. 6 show an increase in grain size under increased SSI, which is attributed to both increases in stronger near-surface temperature gradients (Appendix B in Vionnet et al., 2012) and increased snow temperature (Figure higher snow temperatures during summer (Fig. S4 in supplement) during summer. The absence of a density response to Supplement). Negligible change in simulated density under perturbations in SSI forcing is unclear. In reality, negligible change, or even a decrease, in appears to support the hypothesis of a near-surface density may be attributed to mass loss via sublimation (Inoue et al., 2023). However, vapour transport is not modelled in Crocus and it is therefore more likely that this artifact is linked to the compaction scheme.

The sensitivity of bulk grain size to accumulation rate can be linked to the indirect effect of the grain size mechanism (e.g., Bender, 2002), although this may be due to the absence of vapour transport in the Crocus model. Increased snow metamorphism rate can also explain the increased grain size with increased temperature (Legagneux et al., 2003), while an increase in density

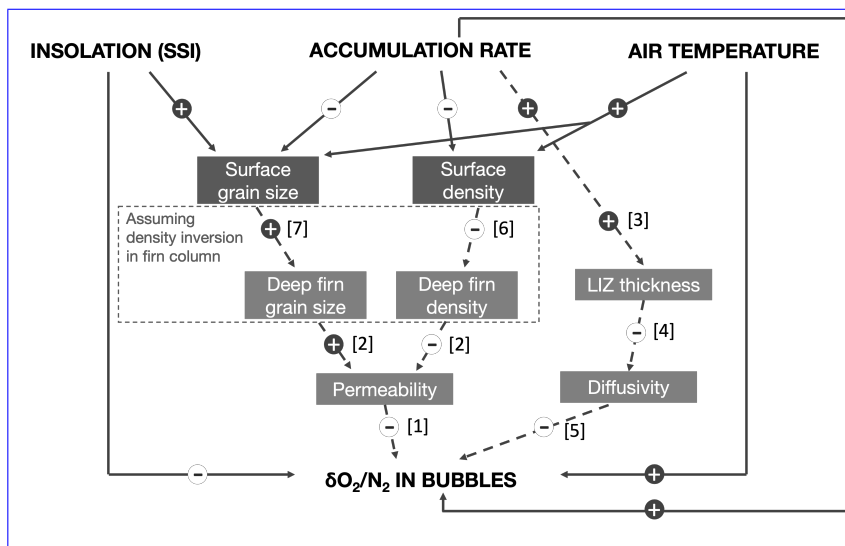


Figure 9. Schematic to show interactions between surface forcings, physical properties, and close-off fractionation. Plus signs show a direct relationship (i.e., increase in SSI corresponds to increase in grain size), and minus signs indicate an inverse relationship. We use full lines to show results from our study, and dashed lines to show links based on previous studies, the numbers for which can be found in the text with associated references.

640 results from increased compaction rates (Vionnet et al., 2012). The decrease in grain size with increased accumulation rate is the result of longer residence time of a snow layer in the upper centimetres to metres of the snowpack, where temperature gradients are strongest (Vionnet et al., 2012; Picard et al., 2012). Shorter residence time with increased accumulation rate (A max) impedes snow metamorphism, resulting in smaller grain size (Picard et al., 2012).

645 It is widely accepted that permeation is the process by which small molecules escape during pore closure (Fig. 9 [1]; e.g., Ikeda-Fukazawa et al., 2004; Huber et al., 2006; Severinghaus and Battle, 2006). Gregory et al. (2014) found that permeability is increased in high-density, and vice versa. A corresponding decrease in snow density under A max facilitates grain growth (Eq. B1 in Vionnet et al., 2012), but this effect is minor compared to the residence time. Increased grain size in T max can be attributed to an increase in the rate of snow metamorphism with temperature, independent of changes in temperature gradient (Legagneux et al., 2003). Large-grained firn due to a less complex pore structure. Indeed, Calonne et al. (2022) showed that grain size has a strong influence on permeability, such that for a given density, permeability is increased with grain size (Fig. 9 [2]). Our results show that high SSI and low accumulation rate are associated with larger grain size and lower $\delta O_2/N_2$. This observation supports the hypothesis that increased SSI (decreased accumulation rate) ultimately leads to lower $\delta O_2/N_2$ due to the increased permeability associated with increased grain size (e.g., Severinghaus and Battle, 2006; Fujita et al., 2009), and suggests a similar mechanism can explain the accumulation rate dependence.

655 Based on the results presented in our study, the anti-correlation between SSI and $\delta O_2/N_2$ is coherent with identifying the mechanisms driving the accumulation rate dependence of $\delta O_2/N_2$ is complicated by the fact that, at polar sites, accumulation rate tends to covary with temperature (Fig. 8). Thus, an increase in near-surface grain size for a given density, leading to bulk ice with decreased grain size with increased near-surface residence time (decreased accumulation rate) will be countered by reduced snow metamorphism rates with a decrease in temperature (Fig. 6). These counteracting effects were invoked by Kawamura et al. (2007) to explain the absence of a 100-ka periodicity in $\delta O_2/N_2$. The opposite—a decrease in grain size for a given density—would thus result in bulk ice with increased records at Dome Fuji. However, the stronger correlation between $\delta O_2/N_2$ and accumulation rate than temperature in Fig. 3 suggests a dominant influence of accumulation rate over temperature, given the decreased grain size under A max conditions. We note, however, that and accumulation rate than temperature in Fig. 3 suggests a dominant role of accumulation. Therefore, we propose that a grain size mechanism—like that of SSI—may explain the positive correlation between accumulation rate and temperature co-vary and thus this interpretation is oversimplified. Regardless, a stronger correlation between $\delta O_2/N_2$ and accumulation rate than temperature in Figure 3 supports the dominant role of accumulation rate at in the EDC core (Fig. 3b).

670 Previous studies propose that firn column characteristics, such as delta-age, will also modulate $\delta O_2/N_2$ via changes in accumulation rate and temperature (Severinghaus and Battle, 2006; Bazin et al., 2016). One mechanism links to the time for pores to close off. At low accumulation sites. However, increased grain growth with temperature (Figure 6) contradicts this interpretation, highlighting a sensitive balance between temperature driven snow metamorphism, and accumulation driven burial rates. Our findings suggest a link between bulk ice, pores will take longer to fully close, and thus, experience more elemental fractionation (Severinghaus and Battle, 2006). Additional hypotheses point to LIZ thickness and pore space geometry (or tortuosity) (e.g., Fujita et al., 2009). Low accumulation sites tend to have thinner LIZs (Fig. 9 [3]; e.g., Landais et al., 2006; Witrant et al., 20

) and less tortuous pore structure in deep firn associated with large, rounded grains (Gregory et al., 2014). Such characteristics are associated with increased gas diffusivity that would facilitate the removal of O₂-enriched gas back to the atmosphere (Fig. 9 [4]). In contrast, at high accumulation sites, the associated decrease in gas diffusivity in the LIZ would lead to a build up of a stagnant air enriched in O₂ resulting in the trapping of gas with relatively high $\delta\text{O}_2/\text{N}_2$ and density-dependent grain size near the surface, but also suggest the importance of snow (Fig. 9 [5]). Alternatively, Hutterli et al. (2009) proposed that varying near-surface temperature gradients under different SSI intensities modulate anisotropy of the snow, as was confirmed by Leinss et al. (2020), leading to vertically elongated pores under high SSI (low accumulation) conditions. They argue that elongated pores facilitate vertical diffusivity in the LIZ, leading to greater fractionation of $\delta\text{O}_2/\text{firn residence time}$, both near the surface, N₂ (Hutterli et al., 2009), an alternative but complimentary mechanism to LIZ thickness.

The aforementioned mechanisms relating to firn column characteristics indicate a positive correlation between $\delta\text{O}_2/\text{N}_2$ and in the LIZ accumulation rate. This is consistent with Fig. 3b but cannot be directly supported by our sensitivity results. Based on the sensitivity tests in Fig. 6, a link to surface density is not clear. We expect that the role of density in modulating $\delta\text{O}_2/\text{N}_2$ derives from the grain size dependence of densification rates invoked by Freitag et al. (2004), providing an additional link between near-surface grain size and $\delta\text{O}_2/\text{N}_2$, as is outlined in the following section.

4.3.2 ~~The role of depth-dependent~~ Depth-dependent variability as a proxy for layering

~~The role of SSI and local climate on deep firn layering is considered by determining the sensitivity of~~ Density stratification in deep firn has also been invoked to modulate $\delta\text{O}_2/\text{N}_2$ variability (Fujita et al., 2009). Results from the Crocus model are used to infer the sensitivity of near-surface density and grain size variability near the surface. Making the link between to perturbations in input forcing parameters. Figure 7 shows that grain size variability is increased with an increase in both SSI and accumulation rate. For SSI, this is expected given enhanced snow metamorphism during summer due to higher snow temperatures (Fig. S4 in Supplement), while winter conditions are largely unchanged. Decreased grain size variability in both the increased and decreased temperature simulations is likely linked to the way in which temperature forcing is perturbed. By applying a constant increase in air temperature, the strength of metamorphism is increased during winter due to higher temperatures (Legagneux et al., 2003; Flanner and Zender, 2006), but largely unchanged during summer due to the dominant influence of insolation on summer snow temperature (Fig. S4), resulting in homogeneity within the snowpack.

Linking variability near the surface and with variability in deep firn is not straightforward/trivial. Indeed, a study by Hörhold et al. (2011) used a compilation of firn cores from numerous polar sites to show that density variability in deep firn is positively correlated with local accumulation rate and temperature, but anti-correlated with near-surface density variability. Although/However, this anti-correlation was not observed by Inoue et al. (2023) when comparing firn cores in the Dome Fuji area where the range of accumulation rate (temperature) was narrower. Additional consideration both from data and modelling approaches is required for density inversions in the firn column -whereby- whereby relatively low-density layers located in the upper part of the firn become relatively high-density layers below the density inversion depth, due to preferential deformation in the upper firn (Freitag et al., 2004; Fujita et al., 2009). Moreover, (Fig. 9 [6]; Freitag et al., 2004; Fujita et al., 2009). Freitag et al. (2004) proposed that the inversion is largely driven by grain size, such that initially low-density layers associated

with large grain size become relatively high-density layers with large grain size below the density inversion (Fig. 9 [7]). This has since been supported by Gregory et al. (2014) who further show that near surface grain size determines the density at which pores close-off. They show that large-grained, high-density layers are more permeable and hence, close off deeper than fine-grained, low-density layers. In addition, Hörhold et al. (2012) suggested that stratification at depth may also be influenced by impurity content, with impurity-rich layers being more susceptible to densification (Hörhold et al., 2012). Given the array of factors proposed to influence deep firn density variability, we focus on the role of grain size variability.

Increased No inversion is observed for grain size variability in SSI max in Figure 7 supports the conclusions of Fujita et al. (2009) that layering is enhanced with SSI due to increased seasonality in snow temperature and temperature gradients, and vice versa. Conversely, decreased grain size. Deep firn layers retain evidence of near-surface grain size, which is determined by snow metamorphism and accumulation rate, as mentioned previously (Gregory et al., 2014). While our sensitivity tests are constrained to the near surface, we draw on previous studies to suggest potential implications for deep firn properties and $\delta O_2/N_2$. Given the presence of a density inversion at Dome C (Hörhold et al., 2011), we may expect that relatively increased variability in near-surface grain size from our sensitivity tests would translate to increased grain size and density variability in the deep firn. As such, increased grain size variability in our SSI max simulation (Fig. 7) supports the conclusions of Fujita et al. (2009), that elemental fractionation is enhanced under high SSI conditions due partially to layering.

The link to accumulation rate is less clear. As for SSI, we observe an increase in grain size variability in both the increased and decreased temperature simulations is likely linked to the way in which temperature forcing is perturbed. By applying a constant increase in air temperature, the strength of metamorphism is increased during winter due to higher temperatures (Legagneux et al., 2003; Flanner and Zender, 2006), while snow temperatures during summer are less effected (Figure S4) — due to the dominant influence of insolation on summer snow temperature. The weaker effect during summer results in homogeneity in the snowpack. Opposingly, a decrease in temperature would suppress metamorphism throughout the year — as evidenced by a decrease in mean grain size (Figure 6) — resulting in relatively decreased variability in the snowpack. The combined influence of accumulation rate and temperature perturbations is expected to result in a complex response in both σ_ρ and σ_{gs} . Moreover, the variability — and bulk mean — differences are likely to be very sensitive to the ascribed glacial and interglacial accumulation rate and temperature values, leading to potentially inaccurate interpretations. This is particularly important for glacial temperature reconstructions which are debated to have been overestimated by up to $5^\circ C$ (Buizert, 2021) with increased accumulation rate. However, according to the layering hypothesis, this should result in more $\delta O_2/N_2$ fractionation at close off, which contradicts our observations of a positive correlation between $\delta O_2/N_2$ and accumulation rate (Fig. 3b). Instead, we suggest that a decrease in mean grain size with increased accumulation rate is dominant over the layering effect. Future work would benefit from an inter site comparison of deep firn properties alongside gas measurements in order to disentangle these effects.

Extracting concrete conclusions from the our variability analysis and extrapolating these into the deep firn is inhibited by both the ascribed forcing perturbations and the aggregation scheme of the model, which is particularly sensitive to changes in accumulation rate. We thus conclude that the simulations performed with the Crocus model can support a mechanism of bulk linked to average grain size on $\delta O_2/N_2$ in ice but not a mechanism implying density or grain size variability. However, our

conclusion does not rule out the effect of layering or grain size variability on $\delta O_2/N_2$ variability but highlights a limitation in our study, as explained in the next section.

4.4 ~~Perspectives~~Limitations and ~~limitations~~perspectives

745 ~~As noted in Section 3.2.1, there is a cold bias in simulated surface temperature compared to observations during summer, which is expected to be consistent between simulations. We therefore argue that this should not influence our qualitative interpretations of the anomalies in density and grain size (relative to the reference), especially considering that Crocus accurately reproduces~~ A number of limitations have been mentioned throughout our study and warrant some further discussion. As mentioned in Section 4.3.2, our study is unable to fully consider the sensitivity of layering to perturbations in forcing parameters. Firstly, near-surface
750 ~~density and grain size profiles (Figure 5). The variability, however, is~~ variability are not fully captured by the model ~~and can be explained by~~ which can be partially attributed to the absence of snow transport by the wind in the standard version of Crocus (Libois et al., 2014). ~~Libois et al. (2014) were able to improve the variability reproducibility in the top 50 cm using a multi-patch approach to account for snow transport by the wind. Further, Inoue et al. (2023) found that wind speed was the major factor controlling density variability from 6 cores near Dome Fuji. While the effects of wind on snow properties are important~~ (Pinzer and Schneebeli, 2009; Dadic et al., 2015; Inoue et al., 2023), the absence of wind transport from our simulations is not expected to influence the results from the sensitivity tests. Moreover, from a paleo-climatological perspective, While wind is known to strongly influence snow properties (e.g. Inoue et al., 2023), we are limited in our understanding of winds throughout the Quaternary. In parallel
755 ~~past 800 ka and therefore wind effects are not considered in our study. Secondly,~~ the aggregation of layers with depth in Crocus make it difficult to focus on both the fine-layered near-surface snow, and the propagation of stratified layers into the deep firn. Accurate assessment of the layering effect would require a new dedicated snow model preserving individual snow layers and properties over a large depth range, from the surface to LIZ, and at high resolution.

~~We also reiterate that accumulation rate depends on temperature which in turn is linked to local SSI. We maintain that~~ While the single-parameter sensitivity tests presented here provide useful insights for understanding physical mechanisms, ~~but they~~ do not account for complex compound effects ~~expected in reality. Indeed, additional tests perturbing multiple forcing parameters associated with the covariance of accumulation rate and temperature at polar sites. Additional tests perturbing both accumulation rate and temperature~~ simultaneously indicate that snowpack properties are very sensitive to the ascribed accumulation rate and temperature values ~~. Because this modelling approach also has weaknesses, as detailed above, we did not use it for interpretation of compound effects in this study.~~

~~A number of commonly proposed mechanisms to explain $\delta O_2/N_2$ variability were considered in our analysis. However,~~ it is important to note that there are other possible explanatory mechanisms. The influence of microstructural properties beyond grain size has not been discussed but poses an alternative mechanistic explanation for elemental fractionation during pore closure. Hutterli et al. (2009) theoretically showed that changes in near-surface temperature gradients under varying climate states modulate the anisotropy of the ice due to variations in temperature gradient metamorphism. This theory was recently confirmed by Leinss et al. (2020) who found that snow anisotropy was predominantly driven by vertical water vapour
775 ~~fluxes in the near-surface snow. Periods of high SSI facilitate temperature gradient metamorphism in the vertical, resulting~~

in elongated pores allowing more fractionation (Hutterli et al., 2009; Leinss et al., 2020). Similarly, low accumulation rates will prolong the residence time of snow layers near the surface where temperature gradients are strongest, thus facilitating snow metamorphism (e.g. Inoue et al., 2023). While assessing pore shape and anisotropy is outside the scope of this study, i.e., for glacial temperature reconstructions which are debated to have been overestimated by up to 5°C (Buizert et al., 2021).
780 Moreover, the additive effects from the single-parameter sensitivity tests (accumulation rate and temperature) do not equal the effects of the direction of change is consistent with our results, such that periods of high accumulation rate, and temperature multi-parameter sensitivity simulations (i.e., would reduce near-surface temperature gradient metamorphism, allowing less fractionation resulting in increased perturbing both accumulation rate and temperature), highlighting the complex influence of quasi-covarying accumulation rate and temperature on snow properties. Given the uncertainties in climatic reconstructions and
785 the limitations mentioned above, we did not attempt to use the model for glacial-interglacial simulations to avoid misinterpreting the results.

Finally, the limited availability and temporal range of $\delta O_2/N_2$ =

We lastly consider the bias towards low accumulation sites in our study. The majority of the datasets included in this study were relatively low-resolution, which limited the analysis of non-orbital temporal variability. While records from Greenland
790 cores meant that our study is slightly biased towards Antarctic sites, which tend to be characterised by low accumulation rates. Although peaks in $\delta O_2/N_2$ corresponding to Dansgaard-Oeschger events are apparent in data from GISP2, which was previously observed by (Suwa and Bender, 2008b) Suwa and Bender (2008b), much of the data was either of too low resolution or influenced by storage gas-loss to perform additional analysis. The limited availability and temporal range of $\delta O_2/N_2$ records from Greenland cores meant that our study is slightly biased towards Antarctic sites, which tend to be characterised by low
795 accumulation rates. Given this bias, we were unable to explore the opposing millennial-scale behaviour observed at low and high accumulation sites for both $\delta O_2/N_2$ and TAC (Kobashi et al., 2015; Eicher et al., 2016). Future studies would therefore benefit from obtaining high resolution measurements from sites with different characteristics.

5 Conclusions

We present a compilation of $\delta O_2/N_2$ records measured on multiple ice cores from Greenland and Antarctica, to improve the
800 mechanistic explanation for $\delta O_2/N_2$ variability. Analysis of both spatial (multi-site) and temporal (single-site) and spatial (multi-site) variability in $\delta O_2/N_2$ revealed presents new evidence of a dependence on local climate (accumulation rate and temperature), in addition to the well-documented insolation dependence. SSI dependence. High resolution measurements from the EDC ice core hinted to a reveals millennial-scale variability in $\delta O_2/N_2$ behaving in-phase with δD records when both parameters are plotted on the AICC2012-AICC2023 ice-age scale. The inter-site analysis revealed showed an increase in mean
805 $\delta O_2/N_2$ for sites with higher accumulation rate and temperature, which is analogous with the temporal analysis from EDC showing $\delta O_2/N_2$ to increase together with δD .

We argue for a dominant suggest that a mechanism relating to firm physical properties mechanism which links can partially explain both the influence of SSI and local climate to on $\delta O_2/N_2$ variability on the ice-age scale by modulating near-surface

~~snow properties~~. Sensitivity tests using the Crocus model show that grain size is very responsive to perturbations in SSI, accumulation rate and air temperature, while density responds to all but SSI perturbations. Our findings support the hypothesis that a grain size mechanism partially controls elemental fractionation during pore closure is the dominant driver of elemental fractionation at low accumulation sites, such that increased grain size for a given density facilitates O₂ expulsion via enhanced permeability. ~~We argue~~ Furthermore, our results support the hypothesis that the presence, or lack thereof ~~at sites such as Dome Fuji (Kawamura et al., 2007)~~, of a local climatic signal in $\delta\text{O}_2/\text{N}_2$ variability is due to the delicate balance between the counter- effects of accumulation rate and temperature on grain properties. However, the inter-site results suggest that low accumulation, low temperature sites experience stronger elemental fractionation, having a comparable effect to high insolation.

While our findings from the $\delta\text{O}_2/\text{N}_2$ data compilation can be supported by the Crocus sensitivity tests, we acknowledge that ~~there may be more complex mechanisms~~ additional mechanisms are at play. In particular, the influence of deep firn layering – itself linked to surface snow metamorphism – could not be tested fully in this study but is believed to play a major role ~~on~~ bulk ice in modulating $\delta\text{O}_2/\text{N}_2$. Determining the relative influence of stratification, firn physical properties, and residence time in the lock-in zone, using ~~firn models~~ a combination of firn models and observations would be useful for future studies.

Code availability. The Crocus model is open-source, and the code is available at https://opensource.umr-cnrm.fr/projects/snowtools_git/wiki/Procedure_for_new_users. The version used is labeled as Surfex V8_1.

Data availability. All unpublished $\delta\text{O}_2/\text{N}_2$ data measured at LSCE will be made available online. Published datasets are available online at the references in Table S2 in the supplement.

Author contributions. AL, EC and FP performed measurements/produced the unpublished datasets measured at LSCE - on ice provided by RM and BS - and CB and JS provided unpublished datasets measured at Scripps. Snow temperature data from Dome C was acquired and shared by LA and GP. RHS ran the Crocus simulations, with the support of MD and QL. RHS and AL prepared the manuscript with contributions from all co-authors.

Competing interests. At least one of the authors is a member of the editorial board of The Cryosphere.

Acknowledgements. This publication was generated in the frame of DEEPICE project. The project has received funding from the European Union's Horizon 2020 research and innovation programme under the Marie Skłodowska-Curie grant agreement No 955750. The measurements leading to these results has also received funding from the European Union's H2020 Programme (H2020/20192024)/ERC grant agreement no. 817493 (ERC ICORDA). EC acknowledges the financial support from the French National Research Agency under the

835 “Programme d’Investissements d’Avenir” (ANR-19-MPGA-0001). MD has received funding from the European Research Council (ERC) under the European Union’s Horizon 2020 research and innovation program (IVORI; grant no. 949516). We also thank Matthieu Fructus for providing his expertise and support in the Crocus model.

Financial support. This research has been supported by the Horizon 2020 research and innovation programme (grant no. 955750 and grant no. 817493).

840 References

- Albert, M., Shuman, C., Courville, Z., Bauer, R., Fahnestock, M., and Scambos, T.: Extreme firn metamorphism: impact of decades of vapor transport on near-surface firn at a low-accumulation glazed site on the East Antarctic plateau, *Annals of Glaciology*, 39, 73–78, <https://doi.org/10.3189/172756404781814041>, 2004.
- Alley, R. B. and Koci, B. R.: Ice-core analysis at site A, Greenland: preliminary results, *Annals of Glaciology*, 10, 1–4, <https://doi.org/10.3189/S0260305500004067>, 1988.
- 845 Alley, R. B., Meese, D., Shuman, C., Gow, A., Taylor, K., Grootes, P., White, J., Ram, M., Waddington, E., Mayewski, P., et al.: Abrupt increase in Greenland snow accumulation at the end of the Younger Dryas event, *Nature*, 362, 527–529, <https://doi.org/10.1038/362527a0>, 1993.
- Arnaud, L., Barnola, J. M., and Duval, P.: Physical modeling of the densification of snow/ firn and ice in the upper part of polar ice sheets, in: *Physics of ice core records*, pp. 285–305, Hokkaido University Press, <http://hdl.handle.net/2115/32472>, 2000.
- 850 Battle, M., Bender, M., Sowers, T., Tans, P., Butler, J., Elkins, J., Ellis, J., Conway, T., Zhang, N., Lang, P., et al.: Atmospheric gas concentrations over the past century measured in air from firn at the South Pole, *Nature*, 383, 231–235, <https://doi.org/10.1038/383231a0>, 1996.
- Battle, M., Severinghaus, J., Sofen, E., Plotkin, D., Orsi, A., Aydin, M., Montzka, S., Sowers, T., and Tans, P.: Controls on the movement and composition of firn air at the West Antarctic Ice Sheet Divide, *Atmospheric Chemistry and Physics*, 11, 11 007–11 021, <https://doi.org/10.5194/acp-11-11007-2011>, 2011.
- 855 Bazin, L., Landais, A., Lemieux-Dudon, B., Toyé Mahamadou Kele, H., Veres, D., Parrenin, F., Martinerie, P., Ritz, C., Capron, E., Lipenkov, V., Loutre, M.-F., Raynaud, D., Vinther, B., Svensson, A., Rasmussen, S. O., Severi, M., Blunier, T., Leuenberger, M., Fischer, H., Masson-Delmotte, V., Chappellaz, J., and Wolff, E.: An optimized multi-proxy, multi-site Antarctic ice and gas orbital chronology (AICC2012): 120ndash;800 ka, *Climate of the Past*, 9, 1715–1731, <https://doi.org/10.5194/cp-9-1715-2013>, 2013.
- 860 Bazin, L., Landais, A., Capron, E., Masson-Delmotte, V., Ritz, C., Picard, G., Jouzel, J., Dumont, M., Leuenberger, M., and Prié, F.: Phase relationships between orbital forcing and the composition of air trapped in Antarctic ice cores, *Climate of the Past*, 12, 729–748, <https://doi.org/10.5194/cp-12-729-2016>, 2016.
- Bender, M., Sowers, T., and Lipenkov, V.: On the concentrations of O₂, N₂, and Ar in trapped gases from ice cores, *Journal of Geophysical Research: Atmospheres*, 100, 18 651–18 660, <https://doi.org/10.1029/94JD02212>, 1995.
- 865 Bender, M. L.: Orbital tuning chronology for the Vostok climate record supported by trapped gas composition, *Earth and Planetary Science Letters*, 204, 275–289, [https://doi.org/https://doi.org/10.1016/S0012-821X\(02\)00980-9](https://doi.org/https://doi.org/10.1016/S0012-821X(02)00980-9), 2002.
- Bender, M. L., Tans, P. P., Ellis, J., Orchardo, J., and Habfast, K.: A high precision isotope ratio mass spectrometry method for measuring the O₂/N₂ ratio of air, *Geochimica et Cosmochimica Acta*, 58, 4751–4758, [https://doi.org/https://doi.org/10.1016/0016-7037\(94\)90205-4](https://doi.org/https://doi.org/10.1016/0016-7037(94)90205-4), 1994.
- 870 Bertler, N. A., Conway, H., Dahl-Jensen, D., Emanuelsson, U., Winstrup, M., Vallelonga, P. T., Lee, J. E., Brook, E. J., Severinghaus, J. P., Fudge, T. J., Keller, E. D., Baisden, W. T., Hindmarsh, R. C. A., Neff, P. D., Blunier, T., Edwards, R. L., Mayewski, P. A., Kipfstuhl, S., Buizert, C., Canessa, S., Dacic, R., Kjær, H. A., Kurbatov, A., Zhang, D., Waddington, E. D., Baccolo, G., Beers, T., Brightley, H. J., Carter, L., Clemens-Sewall, D., Ciobanu, V. G., Delmonte, B., Eling, L., Ellis, A. A., Ganesh, S., Golledge, N. R., Haines, S. A., Handley, M., Hawley, R. L., Hogan, C. M., Johnson, K. M., Korotkikh, E., Lowry, D. P., Mandeno, D., McKay, R. M., Menking, J. A., Naish, T. R., Noerling, C., Ollive, A., Orsi, A. J., Proemse, B. C., Pyne, A. R., Pyne, R. L., Renwick, J., Scherer, R. P., Semper, S.,

- 880 Simonsen, M., Sneed, S. B., Steig, E. J., Tuohy, A., Ulayottil Venugopal, A., Valero Delgado, F., Venkatesh, J., Wang, F., Wang, S., Winski, D. A., Winton, V. H. L., Whiteford, A., Xiao, C., Yang, J., and Zhang, X.: Roosevelt Island Climate Evolution (RICE) ice core isotope record, <https://doi.org/10.1594/PANGAEA.880396>, supplement to: Bertler, NA et al. (2018): The Ross Sea dipole - temperature, snow accumulation and sea ice variability in the Ross Sea region, Antarctica, over the past 2700 years. *Climate of the Past*, 14, 193-214, <https://doi.org/10.5194/cp-14-193-2018>, 2017.
- 885 Bertler, N. A. N., Conway, H., Dahl-Jensen, D., Emanuelsson, D. B., Winstrup, M., Vallelonga, P. T., Lee, J. E., Brook, E. J., Severinghaus, J. P., Fudge, T. J., Keller, E. D., Baisden, W. T., Hindmarsh, R. C. A., Neff, P. D., Blunier, T., Edwards, R., Mayewski, P. A., Kipfstuhl, S., Buizert, C., Canessa, S., Dacic, R., Kjær, H. A., Kurbatov, A., Zhang, D., Waddington, E. D., Baccolo, G., Beers, T., Brightley, H. J., Carter, L., Clemens-Sewall, D., Ciobanu, V. G., Delmonte, B., Eling, L., Ellis, A., Ganesh, S., Golledge, N. R., Haines, S., Handley, M., Hawley, R. L., Hogan, C. M., Johnson, K. M., Korotkikh, E., Lowry, D. P., Mandeno, D., McKay, R. M., Menking, J. A., Naish, T. R., Noerling, C., Ollive, A., Orsi, A., Proemse, B. C., Pyne, A. R., Pyne, R. L., Renwick, J., Scherer, R. P., Semper, S., Simonsen, M., Sneed, S. B., Steig, E. J., Tuohy, A., Venugopal, A. U., Valero-Delgado, F., Venkatesh, J., Wang, F., Wang, S., Winski, D. A., Winton, V. H. L., Whiteford, A., Xiao, C., Yang, J., and Zhang, X.: The Ross Sea Dipole – temperature, snow accumulation and sea ice variability in the Ross Sea region, Antarctica, over the past 2700 years, *Climate of the Past*, 14, 193–214, <https://doi.org/10.5194/cp-14-193-2018>, 2018.
- 895 Bouchet, M., Landais, A., Grisart, A., Parrenin, F., Prié, F., Jacob, R., Fourné, E., Capron, E., Raynaud, D., Lipenkov, V. Y., Loutre, M.-F., Extier, T., Svensson, A., Legrain, E., Martinerie, P., Leuenberger, M., Jiang, W., Ritterbusch, F., Lu, Z.-T., and Yang, G.-M.: The Antarctic Ice Core Chronology 2023 (AICC2023) chronological framework and associated timescale for the European Project for Ice Coring in Antarctica (EPICA) Dome C ice core, *Climate of the Past*, 19, 2257–2286, <https://doi.org/10.5194/cp-19-2257-2023>, 2023.
- Buiron, D., Chappellaz, J., Stenni, B., Frezzotti, M., Baumgartner, M., Capron, E., Landais, A., Lemieux-Dudon, B., Masson-Delmotte, V., Montagnat, M., et al.: TALDICE-1 age scale of the Talos Dome deep ice core, East Antarctica, *Climate of the Past*, 7, 1–16, <https://doi.org/10.5194/cp-7-1-2011>, 2011.
- 900 Buizert, C.: The Ice Core Gas Age-Ice Age Difference as a Proxy for Surface Temperature, *Geophysical Research Letters*, 48, e2021GL094241, <https://doi.org/10.1029/2021GL094241>, 2021.
- Buizert, C. and Severinghaus, J. P.: Dispersion in deep polar firn driven by synoptic-scale surface pressure variability, *The Cryosphere*, 10, 2099–2111, <https://doi.org/10.5194/tc-10-2099-2016>, 2016.
- 905 Buizert, C., Martinerie, P., Petrenko, V., Severinghaus, J., Trudinger, C., Witrant, E., Rosen, J., Orsi, A., Rubino, M., Etheridge, D., et al.: Gas transport in firn: multiple-tracer characterisation and model intercomparison for NEEM, Northern Greenland, *Atmospheric Chemistry and Physics*, 12, 4259–4277, <https://doi.org/10.5194/acp-12-4259-2012>, 2012.
- Buizert, C., Baggenstos, D., Bereiter, B., Bertler, N., Brook, E. J., and Etheridge, D.: Multi-site ice core Krypton stable isotope ratios, <https://doi.org/10.15784/601394>, 2020.
- 910 Buizert, C., Fudge, T., Roberts, W. H., Steig, E. J., Sherriff-Tadano, S., Ritz, C., Lefebvre, E., Edwards, J., Kawamura, K., Oyabu, I., et al.: Antarctic surface temperature and elevation during the Last Glacial Maximum, *Science*, 372, 1097–1101, <https://doi.org/10.1126/science.abd2897>, 2021.
- Buizert, C., Shackleton, S., Severinghaus, J. P., Roberts, W. H. G., Seltzer, A., Bereiter, B., Kawamura, K., Baggenstos, D., Orsi, A. J., Oyabu, I., Birner, B., Morgan, J. D., Brook, E. J., Etheridge, D. M., Thornton, D., Bertler, N., Pyne, R. L., Mulvaney, R., Mosley-Thompson, E., Neff, P. D., and Petrenko, V. V.: The new Kr-86 excess ice core proxy for synoptic activity: West Antarctic storminess

- possibly linked to Intertropical Convergence Zone (ITCZ) movement through the last deglaciation, *Climate of the Past*, 19, 579–606, <https://doi.org/10.5194/cp-19-579-2023>, 2023.
- 915 Calonne, N., Burr, A., Philip, A., Flin, F., and Geindreau, C.: Effective coefficient of diffusion and permeability of firn at Dome C and Lock In, Antarctica, and of various snow types – estimates over the 100–850 kg m⁻³ density range, *The Cryosphere*, 16, 967–980, <https://doi.org/10.5194/tc-16-967-2022>, 2022.
- Capron, E., Landais, A., Chappellaz, J., Schilt, A., Buiron, D., Dahl-Jensen, D., Johnsen, S. J., Jouzel, J., Lemieux-Dudon, B., Loulergue, L., Leuenberger, M., Masson-Delmotte, V., Meyer, H., Oerter, H., and Stenni, B.: Millennial and sub-millennial scale climatic variations recorded in polar ice cores over the last glacial period, *Climate of the Past*, 6, 345–365, <https://doi.org/10.5194/cp-6-345-2010>, 2010.
- 920 Capron, E., Landais, A., Buiron, D., Cauquoin, A., Chappellaz, J., Debret, M., Jouzel, J., Leuenberger, M., Martinerie, P., Masson-Delmotte, V., Mulvaney, R., Parrenin, F., and Prié, F.: Glacial–interglacial dynamics of Antarctic firn columns: comparison between simulations and ice core air- $\delta^{15}\text{N}$ measurements, *Climate of the Past*, 9, 983–999, <https://doi.org/10.5194/cp-9-983-2013>, 2013.
- 925 Carmagnola, C., Morin, S., Lafaysse, M., Domine, F., Lesaffre, B., Lejeune, Y., Picard, G., and Arnaud, L.: Implementation and evaluation of prognostic representations of the optical diameter of snow in the SURFEX/ISBA-Crocus detailed snowpack model, *The Cryosphere*, 8, 417–437, <https://doi.org/10.5194/tc-8-417-2014>, 2014.
- Casado, M., Landais, A., Picard, G., Arnaud, L., Dreossi, G., Stenni, B., and Prié, F.: Water Isotopic Signature of Surface Snow Metamorphism in Antarctica, *Geophysical Research Letters*, 48, e2021GL093382, <https://doi.org/10.1029/2021GL093382>, 2021.
- 930 Champollion, N., Picard, G., Arnaud, L., Lefebvre, E., Macelloni, G., Rémy, F., and Fily, M.: Marked decrease in the near-surface snow density retrieved by AMSR-E satellite at Dome C, Antarctica, between 2002 and 2011, *The Cryosphere*, 13, 1215–1232, <https://doi.org/10.5194/tc-13-1215-2019>, 2019.
- Clow, G. D.: GISP2-D Temperature, <https://doi.org/10.1594/PANGAEA.55517>, 1999.
- Crotti, I., Landais, A., Stenni, B., Bazin, L., Parrenin, F., Frezzotti, M., Ritterbusch, F., Lu, Z.-T., Jiang, W., Yang, G.-M., et al.: An extension of the TALDICE ice core age scale reaching back to MIS 10.1, *Quaternary Science Reviews*, 266, 107078, <https://doi.org/10.1016/j.quascirev.2021.107078>, 2021.
- 935 Cuffey, K. M. and Clow, G. D.: GISP2 accumulation rate history, <https://doi.org/10.1594/PANGAEA.56075>, 1999.
- Cuffey, K. M. and Paterson, W. S. B.: *The physics of glaciers*, Academic Press, 2010.
- Dadic, R., Schneebeli, M., Bertler, N. A., Schwikowski, M., and Matzl, M.: Extreme snow metamorphism in the Allan Hills, Antarctica, as an analogue for glacial conditions with implications for stable isotope composition, *Journal of Glaciology*, 61, 1171–1182, <https://doi.org/10.3189/2015JoG15J027>, 2015.
- 940 Domine, F., Salvatori, R., Legagneux, L., Salzano, R., Fily, M., and Casacchia, R.: Correlation between the specific surface area and the short wave infrared (SWIR) reflectance of snow, *Cold Regions Science and Technology*, 46, 60–68, <https://doi.org/10.1016/j.coldregions.2006.06.002>, 2006.
- 945 Eicher, O., Baumgartner, M., Schilt, A., Schmitt, J., Schwander, J., Stocker, T. F., and Fischer, H.: Climatic and insolation control on the high-resolution total air content in the NGRIP ice core, *Climate of the Past*, 12, 1979–1993, <https://doi.org/10.5194/cp-12-1979-2016>, 2016.
- EPICA community members: Eight glacial cycles from an Antarctic ice core, *Nature*, 429, 623–628, <https://doi.org/10.1038/nature02599>, 2004.
- 950 EPICA community members: One-to-one coupling of glacial climate variability in Greenland and Antarctica, *Nature*, 444, 195–198, <https://doi.org/10.1038/nature05301>, 2006.

- Epifanio, J. A., Brook, E. J., Buizert, C., Pettit, E. C., Edwards, J. S., Fegyveresi, J. M., Sowers, T. A., Severinghaus, J. P., and Kahle, E. C.: Millennial and orbital-scale variability in a 54 000-year record of total air content from the South Pole ice core, *The Cryosphere*, 17, 4837–4851, <https://doi.org/10.5194/tc-17-4837-2023>, 2023.
- 955 Etheridge, D. and Wookey, C.: Ice core drilling at a high accumulation area of Law Dome, Antarctica, 1987, in: *Ice Core Drilling, Proceedings of the Third International Workshop on Ice Core Drilling Technology, Grenoble, France*, pp. 86–96, 1988.
- Etheridge, D. M., Steele, L., Langenfelds, R. L., Francey, R. J., Barnola, J.-M., and Morgan, V.: Natural and anthropogenic changes in atmospheric CO₂ over the last 1000 years from air in Antarctic ice and firn, *Journal of Geophysical Research: Atmospheres*, 101, 4115–4128, <https://doi.org/10.1029/95JD03410>, 1996.
- 960 Extier, T., Landais, A., Bréant, C., Prié, F., Bazin, L., Dreyfus, G., Roche, D. M., and Leuenberger, M.: On the use of $\delta^{18}\text{O}_{\text{atm}}$ for ice core dating, *Quaternary Science Reviews*, 185, 244–257, <https://doi.org/https://doi.org/10.1016/j.quascirev.2018.02.008>, 2018.
- Fegyveresi, J. M., Alley, R., Spencer, M., Fitzpatrick, J., Steig, E., White, J., McConnell, J., and Taylor, K.: Late-Holocene climate evolution at the WAIS Divide site, West Antarctica: bubble number-density estimates, *Journal of Glaciology*, 57, 629–638, <https://doi.org/10.3189/002214311797409677>, 2011.
- 965 Flanner, M. G. and Zender, C. S.: Linking snowpack microphysics and albedo evolution, *Journal of Geophysical Research: Atmospheres*, 111, <https://doi.org/https://doi.org/10.1029/2005JD006834>, 2006.
- Freitag, J., Wilhelms, F., and Kipfstuhl, S.: Microstructure-dependent densification of polar firn derived from X-ray microtomography, *Journal of Glaciology*, 50, 243–250, <https://doi.org/10.3189/172756504781830123>, 2004.
- Frezzotti, M., Pouchet, M., Flora, O., Gandolfi, S., Gay, M., Urbini, S., Vincent, C., Becagli, S., Gragnani, R., Proposito, M., et al.: New
970 estimations of precipitation and surface sublimation in East Antarctica from snow accumulation measurements, *Climate Dynamics*, 23, 803–813, <https://doi.org/10.1007/s00382-004-0462-5>, 2004.
- Fudge, T. J., Buizert, C., Conway, H., and Waddington, E. D.: Accumulation Rates from the WAIS Divide Ice Core, <https://doi.org/110.15784/601004>, 2017.
- Fujita, S., Kawada, K., and Fujii, Y.: Glaciological Data Collected by the 37th Japanese Antarctic Research Expedition during 1996-1997,
975 JARE data reports, 27, 1–46, <https://doi.org/10.15094/00004965>, 1998.
- Fujita, S., Okuyama, J., Hori, A., and Hondoh, T.: Metamorphism of stratified firn at Dome Fuji, Antarctica: A mechanism for local insolation modulation of gas transport conditions during bubble close off, *Journal of Geophysical Research: Earth Surface*, 114, <https://doi.org/https://doi.org/10.1029/2008JF001143>, 2009.
- Gallet, J.-C., Domine, F., and Dumont, M.: Measuring the specific surface area of wet snow using 1310 nm reflectance, *The Cryosphere*, 8,
980 1139–1148, <https://doi.org/10.5194/tc-8-1139-2014>, 2014.
- Gkinis, V., Vinther, B. M., Popp, T. J., Quistgaard, T., Faber, A.-K., Holme, C. T., Jensen, C.-M., Lanzky, M., Lütt, A.-M., Mandrakis, V., et al.: A 120,000-year long climate record from a NW-Greenland deep ice core at ultra-high resolution, *Scientific data*, 8, 141, <https://doi.org/10.1038/s41597-021-00916-9>, 2021.
- Gow, A., Meese, D., Alley, R., Fitzpatrick, J., Anandakrishnan, S., Woods, G., and Elder, B.: Physical and structural properties of the Greenland Ice Sheet Project 2 ice core: A review, *Journal of Geophysical Research: Oceans*, 102, 26 559–26 575, <https://doi.org/10.1029/97JC00165>, 1997.
- 985 Gregory, S. A., Albert, M. R., and Baker, I.: Impact of physical properties and accumulation rate on pore close-off in layered firn, *The Cryosphere*, 8, 91–105, <https://doi.org/10.5194/tc-8-91-2014>, 2014.

- Grenfell, T. C., Warren, S. G., and Mullen, P. C.: Reflection of solar radiation by the Antarctic snow surface at ultraviolet, visible, and near-infrared wavelengths, *Journal of Geophysical Research: Atmospheres*, 99, 18 669–18 684, <https://doi.org/10.1029/94JD01484>, 1994.
- 990 Hamilton, G. S.: Mass balance and accumulation rate across Siple Dome, West Antarctica, *Annals of Glaciology*, 35, 102–106, <https://doi.org/10.3189/172756402781816609>, 2002.
- Hersbach, H., Bell, B., Berrisford, P., Hirahara, S., Horányi, A., Muñoz-Sabater, J., Nicolas, J., Peubey, C., Radu, R., Schepers, D., et al.: The ERA5 global reanalysis, *Quarterly Journal of the Royal Meteorological Society*, 146, 1999–2049, <https://doi.org/10.1002/qj.3803>, 2020.
- 995 Hoffmann, H. M., Grieman, M. M., King, A. C., Epifanio, J. A., Martin, K., Vladimirova, D., Pryer, H. V., Doyle, E., Schmidt, A., Humby, J. D., et al.: The ST22 chronology for the Skytrain Ice Rise ice core—Part 1: A stratigraphic chronology of the last 2000 years, *Climate of the Past*, 18, 1831–1847, <https://doi.org/10.5194/cp-18-1831-2022>, 2022.
- Hörhold, M., Kipfstuhl, S., Wilhelms, F., Freitag, J., and Frenzel, A.: The densification of layered polar firn, *Journal of Geophysical Research: Earth Surface*, 116, <https://doi.org/10.1029/2009JF001630>, 2011.
- 1000 Hörhold, M., Laepple, T., Freitag, J., Bigler, M., Fischer, H., and Kipfstuhl, S.: On the impact of impurities on the densification of polar firn, *Earth and Planetary Science Letters*, 325, 93–99, <https://doi.org/10.1016/j.epsl.2011.12.022>, 2012.
- Huber, C., Beyerle, U., Leuenberger, M., Schwander, J., Kipfer, R., Spahni, R., Severinghaus, J., and Weiler, K.: Evidence for molecular size dependent gas fractionation in firn air derived from noble gases, oxygen, and nitrogen measurements, *Earth and Planetary Science Letters*, 243, 61–73, <https://doi.org/10.1016/j.epsl.2005.12.036>, 2006.
- 1005 Hutterli, M. A., Schneebeli, M., Freitag, J., Kipfstuhl, J., and Röthlisberger, R.: Impact of local insolation on snow metamorphism and ice core records, *Physics of Ice Core Records II*, 68, 223–232, <http://hdl.handle.net/2115/45450>, 2009.
- Huybers, P. and Denton, G.: Antarctic temperature at orbital timescales controlled by local summer duration, *Nature Geoscience*, 1, 787–792, <https://doi.org/10.1038/ngeo311>, 2008.
- Ikeda-Fukazawa, T., Hondoh, T., Fukumura, T., Fukazawa, H., and Mae, S.: Variation in N₂/O₂ ratio of occluded air in Dome Fuji antarctic ice, *Journal of Geophysical Research: Atmospheres*, 106, 17 799–17 810, <https://doi.org/10.1029/2000JD000104>, 2001.
- 1010 Ikeda-Fukazawa, T., Kawamura, K., and Hondoh, T.: Mechanism of Molecular Diffusion in Ice Crystals, *Molecular Simulation*, 30, 973–979, <https://doi.org/10.1080/08927020410001709307>, 2004.
- Ikeda-Fukazawa, T., Fukumizu, K., Kawamura, K., Aoki, S., Nakazawa, T., and Hondoh, T.: Effects of molecular diffusion on trapped gas composition in polar ice cores, *Earth and Planetary Science Letters*, 229, 183–192, <https://doi.org/10.1016/j.epsl.2004.11.011>, 2005.
- 1015 Inoue, R., Fujita, S., Kawamura, K., Oyabu, I., Nakazawa, F., and Motoyama, H.: Evolution of layered density and microstructure in near-surface firn around Dome Fuji, Antarctica, *EGU sphere*, 2023, 1–43, <https://doi.org/10.5194/egusphere-2023-1838>, 2023.
- Jouzel, J., Masson-Delmotte, V., Cattani, O., Dreyfus, G., Falourd, S., Hoffmann, G., Minster, B., Nouet, J., Barnola, J.-M., Chappellaz, J., et al.: Orbital and millennial Antarctic climate variability over the past 800,000 years, *science*, 317, 793–796, <https://doi.org/10.1126/science.1141038>, 2007.
- 1020 Kahle, E., Buizert, C., Conway, H., Epifanio, J., Fudge, T. J., and Jones, T. R.: Temperature, accumulation rate, and layer thinning from the South Pole ice core (SPC14), <https://doi.org/10.15784/601396>, 2020.
- Kawamura, K., Parrenin, F., Lisiecki, L., Uemura, R., Vimeux, F., Severinghaus, J. P., Hutterli, M. A., Nakazawa, T., Aoki, S., Jouzel, J., et al.: Northern Hemisphere forcing of climatic cycles in Antarctica over the past 360,000 years, *Nature*, 448, 912–916, <https://doi.org/10.1038/nature06015>, 2007.
- 1025

- Kawamura, K., Motoyama, H., Goto-Azuma, K., Uemura, R., and Oyabu, I.: Dome Fuji Oxygen Isotope and Dust Data over the past 720 ka, <https://doi.org/https://doi.org/10.25921/zphz-qz79>, 2017.
- Kobashi, T., Ikeda-Fukazawa, T., Suwa, M., Schwander, J., Kameda, T., Lundin, J., Hori, A., Motoyama, H., Döring, M., and Leuenberger, M.: Post-bubble close-off fractionation of gases in polar firn and ice cores: effects of accumulation rate on permeation through overloading pressure, *Atmospheric Chemistry and Physics*, 15, 13 895–13 914, <https://doi.org/10.5194/acp-15-13895-2015>, 2015.
- 1030 Landais, A.: Rapid climate variability in the North Atlantic: the contribution of air isotopes trapped in Greenland ice, Phd thesis, Laboratoire des Sciences du Climat et de l'Environnement [Gif-sur-Yvette], Paris, FR, available at <https://www.theses.fr/2004PA066185>, 2004.
- Landais, A., Chappellaz, J., Delmotte, M., Jouzel, J., Blunier, T., Bourg, C., Caillon, N., Cherrier, S., Malaizé, B., Masson-Delmotte, V., Raynaud, D., Schwander, J., and Steffensen, J. P.: A tentative reconstruction of the last interglacial and glacial inception in Greenland based on new gas measurements in the Greenland Ice Core Project (GRIP) ice core, *Journal of Geophysical Research: Atmospheres*, 108, <https://doi.org/https://doi.org/10.1029/2002JD003147>, 2003.
- 1035 Landais, A., Barnola, J., Kawamura, K., Caillon, N., Delmotte, M., Van Ommen, T., Dreyfus, G., Jouzel, J., Masson-Delmotte, V., Minster, B., Freitag, J., Leuenberger, M., Schwander, J., Huber, C., Etheridge, D., and Morgan, V.: Firn-air $\delta^{15}\text{N}$ in modern polar sites and glacial–interglacial ice: a model-data mismatch during glacial periods in Antarctica?, *Quaternary Science Reviews*, 25, 49–62, <https://doi.org/https://doi.org/10.1016/j.quascirev.2005.06.007>, 2006.
- 1040 Landais, A., Dreyfus, G., Capron, E., Pol, K., Loutre, M. F., Raynaud, D., Lipenkov, V. Y., Arnaud, L., Masson-Delmotte, V., Paillard, D., Jouzel, J., and Leuenberger, M.: Towards orbital dating of the EPICA Dome C ice core using $\delta^{15}\text{N}$, *Climate of the Past*, 8, 191–203, <https://doi.org/10.5194/cp-8-191-2012>, 2012.
- Laskar, J., Robutel, P., Joutel, F., Gastineau, M., Correia, A. C. M., and Levrard, B.: A long-term numerical solution for the insolation quantities of the Earth, *AA*, 428, 261–285, <https://doi.org/10.1051/0004-6361:20041335>, 2004.
- 1045 Lazzara, M. A., Keller, L. M., Markle, T., and Gallagher, J.: Fifty-year Amundsen–Scott South Pole station surface climatology, *Atmospheric Research*, 118, 240–259, <https://doi.org/https://doi.org/10.1016/j.atmosres.2012.06.027>, 2012.
- Lee, J. E., Brook, E. J., Bertler, N. A. N., Buizert, C., Baisden, T., Blunier, T., Ciobanu, V. G., Conway, H., Dahl-Jensen, D., Fudge, T. J., Hindmarsh, R., Keller, E. D., Parrenin, F., Severinghaus, J. P., Vallelonga, P., Waddington, E. D., and Winstrup, M.: An 83 000-year-old ice core from Roosevelt Island, Ross Sea, Antarctica, *Climate of the Past*, 16, 1691–1713, <https://doi.org/10.5194/cp-16-1691-2020>, 2020.
- 1050 Legagneux, L., Cabanes, A., and Dominé, F.: Measurement of the specific surface area of 176 snow samples using methane adsorption at 77 K, *Journal of Geophysical Research: Atmospheres*, 107, ACH–5, <https://doi.org/10.1029/2001JD001016>, 2002.
- Legagneux, L., Lauzier, T., Dominé, F., Kuhs, W. F., Heinrichs, T., and Techmer, K.: Rate of decay of specific surface area of snow during isothermal experiments and morphological changes studied by scanning electron microscopy, *Canadian Journal of Physics*, 81, 459–468, <https://doi.org/10.1139/p03-025>, 2003.
- 1055 Leinss, S., Löwe, H., Proksch, M., and Kontu, A.: Modeling the evolution of the structural anisotropy of snow, *The Cryosphere*, 14, 51–75, <https://doi.org/10.5194/tc-14-51-2020>, 2020.
- Libois, Q., Picard, G., France, J. L., Arnaud, L., Dumont, M., Carmagnola, C. M., and King, M. D.: Influence of grain shape on light penetration in snow, *The Cryosphere*, 7, 1803–1818, <https://doi.org/10.5194/tc-7-1803-2013>, 2013.
- 1060 Libois, Q., Picard, G., Arnaud, L., Morin, S., and Brun, E.: Modeling the impact of snow drift on the decameter-scale variability of snow properties on the Antarctic Plateau, *Journal of Geophysical Research: Atmospheres*, 119, 11,662–11,681, <https://doi.org/https://doi.org/10.1002/2014JD022361>, 2014.

- Libois, Q., Picard, G., Arnaud, L., Dumont, M., Lafaysse, M., Morin, S., and Lefebvre, E.: Summertime evolution of snow specific surface area close to the surface on the Antarctic Plateau, *The Cryosphere*, 9, 2383–2398, <https://doi.org/10.5194/tc-9-2383-2015>, 2015.
- 1065 Lipenkov, V., Raynaud, D., Loutre, M., and Duval, P.: On the potential of coupling air content and O₂/N₂ from trapped air for establishing an ice core chronology tuned on local insolation, *Quaternary Science Reviews*, 30, 3280–3289, <https://doi.org/https://doi.org/10.1016/j.quascirev.2011.07.013>, 2011.
- Lüthi, D., Bereiter, B., Stauffer, B., Winkler, R., Schwander, J., Kindler, P., Leuenberger, M., Kipfstuhl, S., Capron, E., Landais, A., Fischer, H., and Stocker, T. F.: CO₂ and O₂/N₂ variations in and just below the bubble–clathrate transformation zone of Antarctic ice cores, *Earth and Planetary Science Letters*, 297, 226–233, <https://doi.org/https://doi.org/10.1016/j.epsl.2010.06.023>, 2010.
- 1070 Martin, K. C., Buizert, C., Edwards, J. S., Kalk, M. L., Riddell-Young, B., Brook, E. J., Beaudette, R., Severinghaus, J. P., and Sowers, T. A.: Bipolar impact and phasing of Heinrich-type climate variability, *Nature*, pp. 1–5, <https://doi.org/10.1038/s41586-023-05875-2>, 2023.
- Martinerie, P., Lipenkov, V. Y., Raynaud, D., Chappellaz, J., Barkov, N. I., , and Lorius, C.: Air content paleo record in the Vostok ice core (Antarctica): A mixed record of climatic and glaciological parameters, *Journal of Geophysical Research: Atmospheres*, 99, 10 565–10 576, <https://doi.org/https://doi.org/10.1029/93JD03223>, 1994.
- 1075 Martinerie, P., Nourtier-Mazauric, E., Barnola, J.-M., Sturges, W. T., Worton, D. R., Atlas, E., Gohar, L. K., Shine, K. P., and Brasseur, G. P.: Long-lived halocarbon trends and budgets from atmospheric chemistry modelling constrained with measurements in polar firn, *Atmospheric Chemistry and Physics*, 9, 3911–3934, <https://doi.org/10.5194/acp-9-3911-2009>, 2009.
- Massam, A.: Modelling the age–depth and temperature profiles of deep ice cores from the Antarctic Peninsula and the Weddell Sea region, *Phd thesis, University of Durham*, available at <https://nora.nerc.ac.uk/id/eprint/520454/>, 2018.
- 1080 Matsuoka, K., Skoglund, A., and Roth, G.: Quantarctica, <https://doi.org/10.21334/npolar.2018.8516e961>, 2018.
- McDowell, I. E., Albert, M. R., Lieblappen, S. A., and Keegan, K. M.: Local Weather Conditions Create Structural Differences between Shallow Firn Columns at Summit, Greenland and WAIS Divide, *Antarctica, Atmosphere*, 11, 1370, 2020.
- Members, N. C.: Eemian interglacial reconstructed from a Greenland folded ice core, *Nature*, 493, 489–494, <https://doi.org/10.1038/nature11789>, 2013.
- 1085 Mitchell, L. E., Buizert, C., Brook, E. J., Breton, D. J., Fegyveresi, J., Baggenstos, D., Orsi, A., Severinghaus, J., Alley, R. B., Albert, M., Rhodes, R. H., McConnell, J. R., Sigl, M., Maselli, O., Gregory, S., and Ahn, J.: Observing and modeling the influence of layering on bubble trapping in polar firn, *Journal of Geophysical Research: Atmospheres*, 120, 2558–2574, <https://doi.org/https://doi.org/10.1002/2014JD022766>, 2015.
- 1090 Moon, T. A., Fisher, M., Stafford, T., and Thurber, A.: QGreenland (v3), 2023.
- Morgan, V., Wookey, C., Li, J., van Ommen, T., Skinner, W., and Fitzpatrick, : Site information and initial results from deep ice drilling on Law Dome, Antarctica, *Journal of Glaciology*, 43, 3–10, <https://doi.org/10.3189/S0022143000002768>, 1997.
- Mosley-Thompson, E., Paskievitch, J. F., Gow, A. J., and Thompson, L. G.: Late 20th century increase in South Pole snow accumulation, *Journal of Geophysical Research: Atmospheres*, 104, 3877–3886, <https://doi.org/10.1029/1998JD200092>, 1999.
- 1095 Mulvaney, R., Alemany, O., and Possenti, P.: The Berkner Island (Antarctica) ice-core drilling project, *Annals of Glaciology*, 47, 115–124, <https://doi.org/10.3189/172756407786857758>, 2007.
- Mulvaney, R., Abram, N. J., Hindmarsh, R. C., Arrowsmith, C., Fleet, L., Triest, J., Sime, L. C., Alemany, O., and Foord, S.: Recent Antarctic Peninsula warming relative to Holocene climate and ice-shelf history, *Nature*, 489, 141–144, <https://doi.org/10.1038/nature11391>, 2012.
- Mulvaney, R., Triest, J., and Alemany, O.: The James Ross Island and the Fletcher Promontory ice-core drilling projects, *Annals of Glaciology*, 55, 179–188, <https://doi.org/10.3189/2014AoG68A044>, 2014.
- 1100

- Mulvaney, R., Rix, J., Polfrey, S., Grieman, M., Martìn, C., Nehrbass-Ahles, C., Rowell, I., Tuckwell, R., and Wolff, E.: Ice drilling on Skytrain Ice Rise and Sherman Island, Antarctica, *Annals of Glaciology*, 62, 311–323, <https://doi.org/10.1017/aog.2021.7>, 2021.
- Mulvaney, R., Wolff, E. W., Grieman, M. M., Hoffmann, H. H., Humby, J. D., Nehrbass-Ahles, C., Rhodes, R. H., Rowell, I. F., Parrenin, F., Schmidely, L., et al.: The ST22 chronology for the Skytrain Ice Rise ice core–Part 2: An age model to the last interglacial and disturbed deep stratigraphy, *Climate of the Past*, 19, 851–864, <https://doi.org/10.5194/cp-19-851-2023>, 2023.
- 1105 Neff, P. D.: A review of the brittle ice zone in polar ice cores, *Annals of Glaciology*, 55, 72–82, <https://doi.org/10.3189/2014AoG68A023>, 2014.
- NGRIP project members: High-resolution record of Northern Hemisphere climate extending into the last interglacial period, *Nature*, 431, 147–151, <https://doi.org/10.1038/nature02805>, 2004.
- 1110 Oerter, H., Wilhelms, F., Jung-Rothenhäusler, F., Göktas, F., Miller, H., Graf, W., and Sommer, S.: Accumulation rates in Dronning Maud Land, Antarctica, as revealed by dielectric-profiling measurements of shallow firn cores, *Annals of Glaciology*, 30, 27–34, <https://doi.org/10.3189/172756400781820705>, 2000.
- Oyabu, I., Kawamura, K., Uchida, T., Fujita, S., Kitamura, K., Hirabayashi, M., Aoki, S., Morimoto, S., Nakazawa, T., Severinghaus, J. P., and Morgan, J. D.: Fractionation of O₂/N₂ and Ar/N₂ in the Antarctic ice sheet during bubble formation and bubble–clathrate hydrate transition from precise gas measurements of the Dome Fuji ice core, *The Cryosphere*, 15, 5529–5555, <https://doi.org/10.5194/tc-15-5529-2021>, 2021.
- 1115 Oyabu, I., Kawamura, K., Buizert, C., Parrenin, F., Orsi, A., Kitamura, K., Aoki, S., and Nakazawa, T.: The Dome Fuji ice core DF2021 chronology (0–207 kyr BP), *Quaternary Science Reviews*, 294, 107 754, <https://doi.org/10.1016/j.quascirev.2022.107754>, 2022.
- Oyabu, I., Kawamura, K., Fujita, S., Inoue, R., Motoyama, H., Fukui, K., Hirabayashi, M., Hoshina, Y., Kurita, N., Nakazawa, F., Ohno, H., Sugiura, K., Suzuki, T., Tsutaki, S., Abe-Ouchi, A., Niwano, M., Parrenin, F., Saito, F., and Yoshimori, M.: Temporal variations of surface mass balance over the last 5000 years around Dome Fuji, Dronning Maud Land, East Antarctica, *Climate of the Past*, 19, 293–321, <https://doi.org/10.5194/cp-19-293-2023>, 2023.
- 1120 Parrenin, F., Barnola, J.-M., Beer, J., Blunier, T., Castellano, E., Chappellaz, J., Dreyfus, G., Fischer, H., Fujita, S., Jouzel, J., et al.: The EDC3 chronology for the EPICA Dome C ice core, *Climate of the Past*, 3, 485–497, <https://doi.org/10.5194/cp-3-485-2007>, 2007.
- 1125 Parrenin, F., Petit, J.-R., Masson-Delmotte, V., Wolff, E., Basile-Doelsch, I., Jouzel, J., Lipenkov, V., Rasmussen, S., Schwander, J., Severi, M., et al.: Volcanic synchronisation between the EPICA Dome C and Vostok ice cores (Antarctica) 0–145 kyr BP, *Climate of the Past*, 8, 1031–1045, <https://doi.org/10.5194/cp-8-1031-2012>, 2012.
- Petit, J.-R., Jouzel, J., Raynaud, D., Barkov, N. I., Barnola, J.-M., Basile, I., Bender, M., Chappellaz, J., Davis, M., Delaygue, G., et al.: Climate and atmospheric history of the past 420,000 years from the Vostok ice core, Antarctica, *Nature*, 399, 429–436, <https://doi.org/10.1038/20859>, 1999.
- 1130 Petrenko, V. V., Severinghaus, J. P., Brook, E. J., Reeh, N., and Schaefer, H.: Gas records from the West Greenland ice margin covering the Last Glacial Termination: a horizontal ice core, *Quaternary Science Reviews*, 25, 865–875, <https://doi.org/https://doi.org/10.1016/j.quascirev.2005.09.005>, 2006.
- Picard, G., Domine, F., Krinner, G., Arnaud, L., and Lefebvre, E.: Inhibition of the positive snow-albedo feedback by precipitation in interior Antarctica, *Nature Climate Change*, 2, 795–798, <https://doi.org/10.1038/nclimate1590>, 2012.
- 1135 Picard, G., Libois, Q., and Arnaud, L.: Refinement of the ice absorption spectrum in the visible using radiance profile measurements in Antarctic snow, *The Cryosphere*, 10, 2655–2672, <https://doi.org/10.5194/tc-10-2655-2016>, 2016.

- Pinzer, B. R. and Schneebeli, M.: Snow metamorphism under alternating temperature gradients: Morphology and recrystallization in surface snow, *Geophysical research letters*, 36, <https://doi.org/10.1029/2009GL039618>, 2009.
- 1140 Rasmussen, S. O., Abbott, P. M., Blunier, T., Bourne, A., Brook, E., Buchardt, S. L., Buizert, C., Chappellaz, J., Clausen, H., Cook, E., et al.: A first chronology for the North Greenland Eemian Ice Drilling (NEEM) ice core, *Climate of the Past*, 9, 2713–2730, <https://doi.org/10.5194/cp-9-2713-2013>, 2013.
- Raynaud, D., Lipenkov, V., Lemieux-Dudon, B., Duval, P., Loutre, M.-F., and Lhomme, N.: The local insolation signature of air content in Antarctic ice. A new step toward an absolute dating of ice records, *Earth and Planetary Science Letters*, 261, 337–349, <https://doi.org/https://doi.org/10.1016/j.epsl.2007.06.025>, 2007.
- 1145 Rubino, M., Etheridge, D., Trudinger, C., Allison, C., Battle, M., Langenfelds, R., Steele, L., Curran, M., Bender, M., White, J., et al.: A revised 1000 year atmospheric $\delta^{13}\text{C}$ -CO₂ record from Law Dome and South Pole, Antarctica, *Journal of Geophysical Research: Atmospheres*, 118, 8482–8499, <https://doi.org/10.1002/jgrd.50668>, 2013.
- Rubino, M., Etheridge, D. M., Thornton, D. P., Howden, R., Allison, C. E., Francey, R. J., Langenfelds, R. L., Steele, L. P., Trudinger, C. M., 1150 Spencer, D. A., Curran, M. A. J., van Ommen, T. D., and Smith, A. M.: Revised records of atmospheric trace gases CO₂, CH₄, N₂O, and $\delta^{13}\text{C}$ -CO₂ over the last 2000 years from Law Dome, Antarctica, *Earth System Science Data*, 11, 473–492, <https://doi.org/10.5194/essd-11-473-2019>, 2019.
- Schaefer, H., Lourantou, A., Chappellaz, J., Lüthi, D., Bereiter, B., and Barnola, J.-M.: On the suitability of partially clathrated ice for analysis of concentration and $\delta^{13}\text{C}$ of palaeo-atmospheric CO₂, *Earth and planetary science letters*, 307, 334–340, <https://doi.org/10.1016/j.epsl.2011.05.007>, 2011.
- 1155 Schwander, J., Sowers, T., Barnola, J.-M., Blunier, T., Fuchs, A., and Malaizé, B.: Age scale of the air in the summit ice: Implication for glacial-interglacial temperature change, *Journal of Geophysical Research: Atmospheres*, 102, 19483–19493, <https://doi.org/https://doi.org/10.1029/97JD01309>, 1997.
- Severinghaus, J.: Nitrogen and Oxygen Gas Isotopes in the Siple Dome and Byrd Ice Cores, Antarctica [Dataset], <https://doi.org/10.7265/N55X26V0>, 2009.
- 1160 Severinghaus, J.: Low-res d15N and d18O of O₂ in the WAIS Divide 06A Deep Core [Dataset], <https://doi.org/10.7265/N5S46PWD>, 2015.
- Severinghaus, J.: South Pole (SPICECORE) 15N, 18O, O₂/N₂ and Ar/N₂ [Dataset], <https://doi.org/10.15784/601152>, 2019.
- Severinghaus, J. P. and Battle, M. O.: Fractionation of gases in polar ice during bubble close-off: New constraints from firm air Ne, Kr and Xe observations, *Earth and Planetary Science Letters*, 244, 474–500, <https://doi.org/https://doi.org/10.1016/j.epsl.2006.01.032>, 2006.
- 1165 Severinghaus, J. P., Grachev, A., and Battle, M.: Thermal fractionation of air in polar firm by seasonal temperature gradients, *Geochemistry, Geophysics, Geosystems*, 2, <https://doi.org/10.1029/2000GC000146>, 2001.
- Shackleton, S. A.: Tracking Past Changes in Ocean Heat Content with Atmospheric Noble Gases in Ice Cores, Doctoral dissertation, University of California, San Diego, <http://dissertations.umi.com/ucsd:18809>, 2019.
- Sowers, T., Bender, M., and Raynaud, D.: Elemental and isotopic composition of occluded O₂ and N₂ in polar ice, *Journal of Geophysical Research: Atmospheres*, 94, 5137–5150, <https://doi.org/https://doi.org/10.1029/JD094iD04p05137>, 1989.
- 1170 Stenni, B., Proposito, M., Gragnani, R., Flora, O., Jouzel, J., Falourd, S., and Frezzotti, M.: Eight centuries of volcanic signal and climate change at Talos Dome (East Antarctica), *Journal of Geophysical Research: Atmospheres*, 107, ACL–3, <https://doi.org/10.1029/2000JD000317>, 2002.

- 1175 Stenni, B., Jouzel, J., Masson-Delmotte, V., Röthlisberger, R., Castellano, E., Cattani, O., Falourd, S., Johnsen, S., Longinelli, A., Sachs, J.,
et al.: A late-glacial high-resolution site and source temperature record derived from the EPICA Dome C isotope records (East Antarctica),
Earth and Planetary Science Letters, 217, 183–195, [https://doi.org/https://doi.org/10.1016/S0012-821X\(03\)00574-0](https://doi.org/https://doi.org/10.1016/S0012-821X(03)00574-0), 2004.
- Stenni, B., Masson-Delmotte, V., Selmo, E., Oerter, H., Meyer, H., Röthlisberger, R., Jouzel, J., Cattani, O., Falourd, S., Fischer, H., Hoff-
mann, G., Iacumin, P., Johnsen, S., Minster, B., and Udisti, R.: The deuterium excess records of EPICA Dome C and Dronning Maud Land
ice cores (East Antarctica), Quaternary Science Reviews, 29, 146–159, <https://doi.org/https://doi.org/10.1016/j.quascirev.2009.10.009>, cli-
1180 mate of the Last Million Years: New Insights from EPICA and Other Records, 2010.
- Sturrock, G., Etheridge, D., Trudinger, C., Fraser, P., and Smith, A.: Atmospheric histories of halocarbons from analysis of Antarctic firn air:
Major Montreal Protocol species, Journal of Geophysical Research: Atmospheres, 107, ACH–12, <https://doi.org/10.1029/2002JD002548>,
2002.
- Suwa, M. and Bender, M. L.: Chronology of the Vostok ice core constrained by O₂/N₂ ratios of occluded air, and its implication for the Vostok
1185 climate records, Quaternary Science Reviews, 27, 1093–1106, <https://doi.org/https://doi.org/10.1016/j.quascirev.2008.02.017>, 2008a.
- Suwa, M. and Bender, M. L.: O₂/N₂ ratios of occluded air in the GISP2 ice core, Journal of Geophysical Research: Atmospheres, 113,
<https://doi.org/https://doi.org/10.1029/2007JD009589>, 2008b.
- Uchida, T., Duval, P., Lipenkov, V. Y., Hondoh, T., Mae, S., and Shoji, H.: Brittle zone and air-hydrate formation in polar ice sheets, Memoirs
of National Institute of Polar Research. Special issue, 49, 298–305, http://purl.org/coar/resource_type/c_6501, 1994.
- 1190 Uemura, R., Motoyama, H., Masson-Delmotte, V., Jouzel, J., Kawamura, K., Goto-Azuma, K., Fujita, S., Kuramoto, T., Hirabayashi, M.,
Miyake, T., et al.: Asynchrony between Antarctic temperature and CO₂ associated with obliquity over the past 720,000 years, Nature
communications, 9, 961, <https://doi.org/10.1038/s41467-018-03328-3>, 2018.
- Vionnet, V., Brun, E., Morin, S., Boone, A., Faroux, S., Le Moigne, P., Martin, E., and Willemet, J.-M.: The detailed snowpack scheme Crocus
and its implementation in SURFEX v7.2, Geoscientific Model Development, 5, 773–791, <https://doi.org/10.5194/gmd-5-773-2012>, 2012.
- 1195 Warming, E., Svensson, A., Vallelonga, P., and Bigler, M.: A technique for continuous detection of drill liquid in ice cores, Journal of
glaciology, 59, 503–506, <https://doi.org/10.3189/2013JoG12J124>, 2013.
- Warren, S. G., Brandt, R. E., and Grenfell, T. C.: Visible and near-ultraviolet absorption spectrum of ice from transmission of solar radiation
into snow, Appl. Opt., 45, 5320–5334, <https://doi.org/10.1364/AO.45.005320>, 2006.
- Watanabe, O., Shimada, W., Narita, H., Miyamoto, A., Tayuki, K., Hondoh, T., Kawamura, T., Fujita, S., Shoji, H., Enomoto, H., et al.: Pre-
1200 liminary discussion of physical properties of the Dome Fuji shallow ice core in 1993, Antarctica, in: Proceedings of the NIPR Symposium
on Polar Meteorology and Glaciology, vol. 11, pp. 1–8, , http://purl.org/coar/resource_type/c_6501, 1997.
- Watanabe, O., Kamiyama, K., Motoyama, H., Fujii, Y., Shoji, H., , and Satow, K.: The paleoclimate recorded in the ice core from Dome Fuji
station, Antarctica, Journal of Geophysical Research: Atmospheres, 29, 176—183, <https://doi.org/10.3189/172756499781821553>, 1999.
- White, J., Bradley, E., Garland, J., Jones, T. R., Morris, V., Price, M., and Vaughn, B.: Stable Isotopes of Ice in the Transition and Glacial
1205 Sections of the WAIS Divide Deep Ice Core, <https://doi.org/10.15784/601274>, 2019.
- Winstrup, M., Vallelonga, P., Kjær, H. A., Fudge, T. J., Lee, J. E., Riis, M. H., Edwards, R., Bertler, N. A. N., Blunier, T., Brook, E. J.,
Buizert, C., Ciobanu, G., Conway, H., Dahl-Jensen, D., Ellis, A., Emanuelsson, B. D., Hindmarsh, R. C. A., Keller, E. D., Kurbatov, A. V.,
Mayewski, P. A., Neff, P. D., Pyne, R. L., Simonsen, M. F., Svensson, A., Tuohy, A., Waddington, E. D., and Wheatley, S.: A 2700-year
annual timescale and accumulation history for an ice core from Roosevelt Island, West Antarctica, Climate of the Past, 15, 751–779,
1210 <https://doi.org/10.5194/cp-15-751-2019>, 2019.

Witrant, E., Martinerie, P., Hogan, C., Laube, J., Kawamura, K., Capron, E., Montzka, S., Dlugokencky, E., Etheridge, D., Blunier, T., et al.: A new multi-gas constrained model of trace gas non-homogeneous transport in firn: evaluation and behaviour at eleven polar sites, *Atmospheric Chemistry and Physics*, 12, 11 465–11 483, <https://doi.org/10.5194/acp-12-11465-2012>, 2012.